4.0 LABORATORY TESTING PROGRAM

4.1 Introduction

An objective of this research is to gain insight into the mechanisms responsible for aging effects in sands. A review of case studies and proposed mechanisms from the literature shows that there is still considerable disagreement and uncertainty over what causes these effects. Presently there is no unambiguous evidence that proves that the mechanisms are mechanical, chemical, some combination of the two, or something completely different. To contribute to the current knowledge of aging effects in sands, a laboratory testing program was developed as a fundamental study of the aging phenomenon.

Specifically, a testing program was designed to produce aging effects and to study the influence of different variables on the presence and magnitude of aging effects. Three different sands were tested in rigid wall cells and five-gallon buckets. Samples were aged under different effective stresses, densities, temperatures, and pore fluids. In every rigid wall cell, three independent measurements were made to monitor property changes during the aging process: small strain shear modulus using bender elements, electrical conductivity, and mini-cone penetration resistance. These measurements were chosen to elucidate the cause of aging effects in sands, and details of each are presented herein.

An overview of the testing program that was performed in the rigid wall cells is as follows:

- Saturated samples were prepared at two different densities and with four different pore fluids.
- Sample preparation involved pluviating sand through a pore fluid and vibrating the loose samples until a desired density was reached.
- Samples were loaded under K_o conditions and allowed to age at two different temperatures.

- Aging effects were monitored during the tests by making small strain shear modulus measurements using bender elements and electrical conductivity measurements of the sample and pore fluid.
- At the end of each test, a mini-cone penetration test was performed. These results were compared to the results of tests performed on identically prepared samples with no period of aging.
- Mineralogical studies were performed after each test to monitor changes in the chemistry of the pore fluid and to look for the presence of precipitation on the sand grains.

Tests were also performed using 5 gallon buckets, which contained saturated sand with different pore fluids. Aging was assessed using mini-cone penetration tests at different location and at different times.

This chapter contains background information on each measurement, the procedures for the laboratory testing program, and the schedule of tests that was accomplished. Details regarding the sands used and equipment details are also presented.

4.2 Equipment Setup

For any study involving time as a variable, it is important to be able to test more than one sample at once. For this study, equipment was constructed such that eight samples in rigid wall cells could be tested simultaneously. This section describes the construction of the rigid wall cells, as well as the load frames and temperature baths used to control stress and temperature conditions.

4.2.1 Rigid Wall Cells

A diagram of the rigid wall cells used in this study is shown in Figure 4.1. Each cell consists of a cell wall, base plate, and top cap. Originally, PVC pipe was used for the cell walls, but this was changed to a composite steel-PVC cell. The composite cell walls had

an inside diameter of 14.5 cm and an outside diameter of 17 cm. The height of the cell walls was 22.4 cm, and the height of the samples tested were, on average, 16.2 cm.

The original PVC cells were constructed of Schedule 80, 6 inch nominal diameter PVC pipe (14.5 cm I. D., 1.1 cm wall thickness). PVC was chosen because it is a good electrical insulator, which was necessary for the electrical conductivity measurements, and it is chemically inert. In order to maintain K_o, or zero lateral strain conditions, steel hose clamps were wrapped around each cell wall along its full length to provide additional stiffness. However, measurements of the small strain shear modulus during the first aging tests at 40^o C showed erratic behavior, and it was discovered that the PVC cell walls were creeping. Figure 4.2 shows the amount of creep, shown as the increase in radial strain with time, for a PVC cell compared to a steel cell with the same dimensions. This information was obtained by installing strain gauges on the outside of each cell wall and loading samples in each cell to a vertical stress of 100 kPa at a temperature of 40^o C.

Based on this information, it was apparent that a stiffer cell wall was needed; however, it was still necessary to use a non-conductive material so the electrical conductivity tests could be performed. It was decided to construct composite cell walls consisting of a PVC sleeve surrounded by a steel jacket. Schedule 80 6 inch diameter PVC pipe and a steel pipe (15.9 cm I. D., 0.5 cm wall thickness) were used. The outer diameter of the PVC pipe was turned down on a lathe to within a few hundredths of a millimeter of the I. D. of the steel pipe. The PVC pipe was then press-fit into the steel pipe in a load frame. The inside of the steel pipe was coated with a fast drying epoxy just prior to being press-fit with the PVC to improve the bond between the two pipes and to fill any possible gaps. Figures 4.3 and 4.4 show the construction of the composite cells. Figure 4.3 shows turning down the PVC pipe on a lathe to fit into the steel shell. Figure 4.4 shows the PVC pipe being press-fit into the steel pipe.

The top caps and base plates for each cell were constructed of 2.54 cm thick, Type I PVC. As shown in Figure 4.1, bender elements and conductivity electrodes were installed in both top caps and base plates, and details of their construction are given in sections 4.4.1.4 and 4.4.2.4, respectively. Two holes were drilled through each top cap so that mini-cone penetration tests could be performed through the caps without unloading the specimens. A 3.6 cm diameter porous stone connected to a drainage port was installed in each base plate.

To prevent the cells from leaking, the cell walls were glued into the base plates using RTV 630, a two-part silicon compound produced by GE Silicones. In order to minimize rusting of the steel portion of the composite cells when placed in water baths, the outside of the cells were coated with a rubberized plastic coating call Rubberize-It produced by DIY.

The settlement measurement system for each cell is shown in Figure 4.5. A dial gauge was attached to a threaded rod that was screwed into the base plate of each sample. The dial gauge rested on 2.0 cm diameter, 5.0 cm high acrylic settlement post, which was screwed into the top cap in one of the two mini-cone penetration test holes. In this way, the vertical settlements of the top cap could be measured without the dial gauge being immersed in the pore fluid of the sample. In addition, this system removes the effect of deflections of the load frame due to the loading of other cells.

4.2.2 Load Frames

Figure 4.6 shows the two steel load frames that were constructed for this study. Each frame is 1.8 m long, 1.0 m high, and 0.8 m wide, and each can load four cells independently in one-dimensional compression. The load frame in the foreground of the figure contains four cells immersed in a water bath, which is covered with white Styrofoam for insulation. Vertical load was applied to the samples with a simple system using either 10:1 or 8:1 lever arms, as shown in Figure 4.7. Load was transferred from

the lever arm to the sample through a 2.54 cm diameter ball bearing resting on the top cap. To prevent the development of shear forces on the top cap as the lever arm rotated during settlement, a greased linear motion bearing (sandwiched between stainless steel washers and heat-sealed in plastic) was placed in between the ball bearing and the top cap. This is shown in Figure 4.8. Weights, which were constructed by melting scrap lead into molds, were hung from hangars at the ends of the lever arms to achieve the desired vertical loads on the samples. In order to minimize disturbance of the samples from ambient vibrations, each load frame was mounted on a sheet of 0.64 cm thick plywood on top of a 0.3 cm thick sheet of cork.

4.2.3 Constant Temperature Water Baths

The samples in each load frame were kept at a constant temperature throughout the aging process. This was accomplished by immersing the cells in water baths, which were constructed of 0.95 cm thick sheets of Type I PVC. Each water bath was heated with a 300 Watt immersion heater (Omega model VP-311) and temperature controller (Omega CN800), and the water was circulated using an aquarium pump (Powerhead 201 produced by Hagen). There was no contact between the pore fluid of the samples and the water in the baths. The rooms in which the laboratory testing program was performed were not climate controlled, however, the baths were able to maintain a constant temperature +/-1^{o} C for up to 118 days. The temperatures within the samples were measured with a copper/constantan thermocouple, which was installed along the inside of the cell wall through the top cap after the sample was prepared.

4.3 Properties of Sands Tested

Three sands were used in this study: Evanston sand, Density sand, and Lightcastle sand. Evanston and Density sand were used for all of the rigid wall tests, whereas Evanston and Lightcastle sand were used for the bucket tests. Grain size distributions for all three sands are shown in Figure 4.9, and relevant soil properties are shown in Table 4.1. All three sands had less than 1% fines, with no clay fraction.

Table 4.1 Properties of sands used in this study.

Sand	D_{50}[1] (mm)	C_u	C_c	γ_{dmin}[2] (kN/m^3)	γ_{dmax}[3] (kN/m^3)	USCS Designation
Evanston Sand	0.30	1.82	1.18	14.5	17.3	SP
Density Sand	0.50	1.93	1.04	15.1	17.5	SP
Lightcastle Sand	0.35	1.82	1.02	13.9	16.6	SP

1. Sieve analysis performed according to ASTM D422.
2. Test performed according to ASTM D4254, Method B.
3. Test performed according to ASTM D4253.

The Evanston sand is a tan, sub-angular, poorly graded fine beach sand obtained from the campus of Northwestern University in Evanston, Illinois. It was chosen specifically for this study because Dowding and Hryciw (1986) observed aging effects with this sand in their laboratory blasting experiments, which was discussed in section 2.4.6. As a natural beach sand, it contained trace amounts of shells and organics. For all the tests, the sand was air-dried and sieved through a No. 10 sieve to remove the large shell fragments, twigs, seaweed, etc. Figure 4.10 shows scanning electron micrographs (SEM) of Evanston sand. The sub-angular nature of the sand can be seen from the figures.

A bulk chemical analysis was also performed on the Evanston sand, and the results are shown in Table 4.2. The constituents of the sand are shown both as percent by weight and the mole fraction. For determining the mineralogy of the Evanston sand, the mole fraction is more illustrative. Since 78.6% of the moles are SiO_2, the sand is primarily composed of quartz. The bulk analysis also suggests there is some carbonate material in the sand, from the presence of CaO and MgO, and trace amounts of potassium feldspar, from the presence of Na_2O and K_2O.

The carbonate material is most likely dolomite, which has the chemical equation $CaMg(CO_3)_2$. This is also supported by the 7.45% of the moles that were lost on ignition.

Most of this is probably CO_2 gas that was freed when the dolomite was broken down during the test. The fact that the mole fraction lost on ignition is greater than both the calcium and magnesium oxides is probably due to the trace amounts of organic material present in the sand.

The presence of carbonate material was verified by immersing the sand in 1 N hydrochloric acid, which caused the carbonate to dissolve and generate carbon dioxide bubbles. Grains of carbonate material were also observed using energy dispersive spectrum analysis (EDS) in conjunction with the SEM. Figure 4.11 (a) shows the results of the EDS on the lower left grain shown in Figure 4.10 (b). The characteristic peaks indicate that the grain is composed of calcium and magnesium, and is probably dolomite. In contrast, Figure 4.11 (b) shows the results of the EDS on the upper right grain shown in Figure 4.10 (b). The strong silica peak indicates that the grain is composed of quartz.

Table 4.2 Bulk chemical analyses of Evanston and Density sand.

	Evanston Sand		Density Sand	
	Weight Fraction (%)	Mole Fraction (%)	Weight Fraction (%)	Mole Fraction (%)
SiO_2	79.1	78.6	98.7	99.4
Al_2O_3	3.56	2.08	.13	0.08
CaO	5.08	5.42	.06	0.07
MgO	2.76	4.11	0	0
Na_2O	.73	0.71	0	0
K_2O	1.06	0.66	0	0
Fe_2O_3	2.11	0.77	1.03	0.39
MnO	.03	0.02	0	0
TiO_2	.251	0.18	.07	0.05
P_2O_5	.03	0.01	0	0
Cr_2O_3	.08	0.03	.13	0.05
Loss on Ignition	5.5	7.45	0	0

Density sand is a commercial quartz sand available from Humbolt, Inc. and is used for sand cone density tests. It is a white, rounded, poorly graded, fine to medium sand, and it was chosen because it is almost purely quartz. In this way, any possible chemical effects during aging for Density sand would have to be due to the dissolution and precipitation of silica only. Figure 4.12 shows scanning electron micrographs of the Density sand. The rounded nature of the sand can be seen from the micrographs. Figure 4.13 shows the EDS results from the one grain from Figure 4.12 (b), which clearly shows the presence of quartz. The bulk chemistry of the Density sand is shown in Table 4.2, which also indicates that it is a purely quartz sand (98.7% moles being SiO_2).

Lightcastle sand is a locally available processed sand from Newcastle, Virginia. It was used only for the bucket tests because large quantities were readily available. It is a brown, poorly graded fine to medium quartz sand. Figure 4.14 shows scanning electron micrographs of the Lightcastle sand. No other mineralogical studies of this sand were performed.

4.4 Test Measurements

In each rigid wall cell, three independent measurements were performed to assess the potential aging effects. These were small strain shear modulus measurements using bender elements, electrical conductivity measurements, and mini-cone penetration tests. In this section, each type of measurement is discussed, including its applicability for monitoring the aging process, some background information, and details of the apparatus that was constructed.

4.4.1 Small Strain Shear Modulus Measurements Using Bender Elements

The stiffness of soils is often measured by the tangent shear modulus obtained from stress-strain relationships. At strains within the elastic range, typically 10^{-4}% or less, the stiffness is represented by the small strain shear modulus, G_o. This parameter is very important in soil structure interaction problems and earthquake engineering where it is

necessary to know how the shear modulus degrades from its small strain value as the level of shear strain increases.

As discussed in section 2.2, the small strain shear modulus can be determined from the theory of elasticity, and can be written as

$$G_o = \rho v_s^2 \qquad (2.2)$$

where

G_o = small strain shear modulus

ρ = mass, or total, density

v_s = shear wave velocity

A shear wave is an elastic body wave, meaning it is a wave that travels within an elastic medium, whose direction of propagation is perpendicular to its direction of particle displacement. A compression wave is another type of elastic body wave, however, its direction of propagation is parallel to its direction of particle displacement.

Although both types of body waves can propagate through soils, the shear wave exhibits some properties that make it more applicable for studying soils. First, in a saturated soil (a two-phase porous medium), shear waves propagate only through the solid phase, because water can not support shear stresses. However, water can support compressive stresses and, for fully saturated undrained conditions, the soil can be considered to be incompressible. Thus, compression waves propagating through a soil travel through both the solid and water phase. This means that the compression wave velocity is heavily dependent on the water in the pores of the soil. In fact, for fully saturated conditions, the water is incompressible compared to the soil skeleton, and the compression waves travel almost exclusively through the water phase. The resulting compression wave velocity in this case equals the compression wave velocity of water.

One method for determining the small strain shear modulus of soils in the laboratory is to propagate a shear wave through a specimen, measure its velocity, and calculate the small strain shear modulus using Equation 2.2. Shear waves can be generated and measured by small pieces of piezoceramic called bender elements, which can be installed in the end caps of specimens. Piezoceramics have the ability to convert electrical impulses to mechanical impulses and vice versa. When a voltage impulse is applied across a single sheet of piezoceramic, it will either shorten or lengthen with a corresponding increase or decrease in thickness, as illustrated in Figure 4.15(a). If two piezoceramic sheets are mounted together with their respective polarities opposite to each other, as shown in Figure 4.15(b), an electrical impulse will cause one side to lengthen and the other side to shorten. The net result of this will be a bending of the two sheets, hence the name bender elements.

Thus, if an electrical impulse is sent to a bender element mounted in the top cap of a specimen, the bender element will produce a small "wiggle" and generate a shear wave that will propagate down through the soil. When the shear wave reaches the bottom of the specimen it will cause the bender element mounted in the bottom cap to vibrate slightly, thus creating an electrical impulse. If an oscilloscope is used to observe both the impulse that was sent to the top bender (transmitter) and the impulse that was generated by the bottom bender element (receiver), the time that it took the wave to propagate can be measured directly, and is called the arrival time. A schematic of this is shown in Figure 4.16. If the length the wave traveled, usually considered to be the length of the sample minus the length of the bender elements (tip-to-tip distance), the shear wave velocity can be calculated by dividing this length (L) by the travel time (Δt), or

$$v_s = \frac{L}{\Delta t} \tag{4.1}$$

4.4.1.1 Motivation for Measuring the Small Strain Shear Modulus during Aging

Because shear waves propagate exclusively through the soil skeleton, they are directly influenced by the behavior of the particle contacts. Different types of interparticle contacts, such as elastic, viscoplastic, and brittle contacts, directly influence the magnitude of the measured shear wave velocity (Cascante and Santamarina 1996; Hardin and Richart 1963). This, along with the fact that, as shown in chapter 2, the small strain shear modulus of clean sands increases with time, makes shear wave velocity measurements a good method for trying to determine the mechanism(s) responsible for aging effects. Most of the mechanisms that are cited in chapter 3 involve changes at the contacts between particles. Dissolution and precipitation of solutes, increased interlocking and pressure solution could all affect measured shear wave velocities. With a well-designed laboratory testing program, some of these potential mechanisms may be eliminated or confirmed.

In addition, generating shear waves and measuring the small strain shear modulus does not change the properties of the samples, and is thus considered to be a non-destructive test. Therefore, small strain shear modulus measurements can be made throughout testing to monitor both the presence and magnitude of aging.

4.4.1.2 Influence of Cementation on the Small Strain Shear Modulus

Acar and El-Tahir (1986) studied the effect of artificial cementation on the small strain shear modulus of Monterey No. 0 sand. Resonant column tests were performed on specimens of different relative densities mixed with 1, 2, and 4% Portland cement. As shown in Figure 4.17, increasing the amount of cement caused an increase in the small strain shear modulus. This increase was reflected by an increase in the coefficient C_g described above and appeared to be independent of the stress dependent coefficient, n. It was also found that the increase in small strain shear modulus was higher for the dense specimens compared to loose specimens.

4.4.1.3 Equipment Details

Figure 4.16 shows a schematic of the equipment for determining the shear wave velocity using bender elements. There are three important components for a good bender element setup: the digital oscilloscope, function generators, and the bender elements.

The important aspects of an oscilloscope for the study of shear waves through soils include the sampling rate, resolution, and storage capabilities. Brignoli et al. (1996) suggest that a minimum sampling rate of 20 x 10^6 samples per second is necessary for accurate shear wave velocity measurements. Typical sampling rates for new digital oscilloscopes are 100 x 10^6 samples per second and are sufficient for testing soils at frequencies less than 100 kHz.

The resolution of the oscilloscope, meaning the smallest voltage signal that can be accurately observed, is extremely important. The received signal of the shear wave velocity is very small, usually between 0.1 and 5 mV. Using an oscilloscope with good resolution (significantly less than the received signal) can remove the need for complicated post-processing techniques such as stacking (adding signals to increase the voltage of the received signal) or using amplifiers on the received signal. It is also important for the oscilloscope to be able to store and download received signals so the signals can be stored for future use or processing.

Three different digital oscilloscopes were used in the development of apparatus for this study. The first, a BK Precision 2520, had a resolution of ~2 mV and only outputted to a strip chart recorder. Both of these features made interpretation of the data difficult, so a second oscilloscope, a Tektronix 468 was used. This oscilloscope had a resolution of ~0.1 mV and had the ability to capture signals and download them through a RD232 port to a data acquisition card in a computer. The third oscilloscope obtained was a Tektronix 430A, which had a resolution of ~10 μV and an internal disk drive so that either bitmap images of the recorded signals or the actual time data could be stored directly to a disk.

This oscilloscope was significantly better than the other two, and the bulk of the data presented herein was obtained using the Tektronix 430A digital oscilloscope.

Two function generators were used in this study: one to act as a triggering mechanism and the other to send a signal to the bender element transmitting the shear wave. This setup follows suggestions made by Dr. Mike Riemer at the University of California at Berkeley. The waveforms generated by the two function generators are illustrated in Figure 4.18. The first function generator, a BK Precision 3011B, generated a low frequency (60 Hz) square wave to synchronize the second function generator, a HP 3312A, and the digital oscilloscope. Every change in polarity of the square wave triggered the HP to send a signal to one of the bender elements and the oscilloscope to start recording the transmitted and received signals.

With the HP function generator, it was possible to send a number of different input signals to the transmitting bender element, including square waves, sine waves, half sine waves, and high frequency pulses. All of these techniques have been successfully used by other researchers, and all were tried in the course of this research. It was found that the half sine wave resulted in the clearest received signals, and it was used throughout this testing program.

The half sine wave that was sent to the transmitting bender elements had an amplitude of 20 V. This was the maximum voltage that could be outputted from the function generator. In general, a larger input signal results in a larger received signal, which usually makes interpretation of the signal easier. For this setup, an input signal of 20 V resulted in a received signal of 0.1 to 3 mV. Larger received signals can be obtained using amplifiers; however, this was not necessary because the resolution of the Tektronix 430A was good enough to clearly measure the received signal.

During the tests, the frequency of the inputted half sine wave was adjusted until the received signal had an optimal amplitude and shape. This is common practice in tests using bender elements, and the optimum excitation frequency of the received signal is a function of the soil and cell rigidity, and the type and arrangement of the bender elements being used (Brignoli et al. 1996).

The bender elements were purchased from Piezo Systems, Inc. of Cambridge, Massachusetts. They can be bought in sheets up to 3.81cm x 6.35 cm, or pre-cut to any size. Initially, a sheet was purchased and cut into 1 cm squares here at Virginia Tech using a diamond table saw. However, the cutting process left rough edges on the bender elements and appeared to distort the received signals, which made interpretation of the arrival time difficult. New, pre-cut bender elements were purchased, which functioned much better and were installed in all eight of the rigid wall cells.

Because the amplitude of the received signal is very small, it is critical that electrical noise be minimized. For this reason, the wiring of the bender elements is very important, and 0.318 cm coaxial cable was used. Dyvik and Madshus (1985) identified two different possible wiring setups for bender elements: a series connection and a parallel connection. These are shown in Figure 4.19. The series connection has a positive and negative lead attached to either piezoceramic sheet. The parallel connection has two positive leads attached to the piezoceramic sheets with the negative lead attached to the steel shim mounted in between. This is significantly more difficult to fabricate because a portion of the piezoceramic material must be ground away to access the steel shim. Dyvik and Madshus reported that the parallel connection was more effective for transferring electrical impulses to mechanical impulses, and the series connection was more effective converting mechanical energy to electrical signals. Thus, the parallel connection is reported to be better for a transmitting bender element, while the series connection is better suited for a receiver. Both types of wiring were tried, however the

parallel connection did not show any different response from the series connection. Thus, all the bender elements in the rigid wall cells were wired with a series connection.

The wires of the coaxial cable were soldered onto the base of each bender element. A special flux, called Superior Flux No. 67 DSA, obtained from Piezosystems, Inc., was required to attach solder to the piezoceramic. Because the bender elements operate by creating or recording a voltage drop across the two piezoceramic sheets, the presence of water will short circuit the system. It is thus imperative to coat the bender elements with a good waterproofing material, especially for long term tests. A two-part epoxy made by 3M called Scotchcast Electrical Resin No. 5 was used, and the bender elements and exposed wiring were completely coated. The thickness of the bender elements was 0.6 mm and after the epoxy was applied the thickness was approximately 2.0 mm. The flux and the waterproofing materials performed well.

The coated bender elements were set into 3 mm wide, 8 mm deep slots that were cut into the top caps and base plates of the cells. They were glued into position using a flexible silicon compound, RTV 630A. Approximately half of the length of the bender elements, or 5 mm, protruded into the samples.

Care was taken to minimize electrical noise from such sources as the fluorescent lights, the heaters, and random noise from the wall outlets. Considerable electrical noise was found to be due to the presence of the electrical conductivity electrodes, which seemed to act as antennae within the cells. Connecting the bender elements, the conductivity electrodes, the function generators, and the oscilloscope to a common ground removed much of this noise.

An image captured from the screen of the digital oscilloscope is shown in Figure 4.20. The vertical axis is a voltage amplitude and the horizontal axis is time in milliseconds. Figure 4.19 shows both the 20 V half sine wave that was sent to the transmitting bender

element (A-B) and the 2 mV (peak-to-peak) received signal (A'-B'). The arrival time of 716 μs was determined by measuring the time difference between the peak of the transmitted signal to the first peak of the received signal, shown as points B and B'. The true time of propagation should be measured from the first deviation from the horizontal for both the transmitted and received signals, shown as points A and A'. However, the peak-to-peak distance was chosen for three reasons:

1. The peak-to-peak distance is much easier to measure, thus simplifying interpretation of the data. The first deviation of the received signal can be very difficult to determine due to the presence of electrical noise.
2. Using the peak-to-peak distance only introduces a small error in the measured shear wave velocity (Arulnathan et al. 1998).
3. For studying the time-dependent properties of sands, changes in the shear wave velocity, and thus the small strain shear modulus, are important. Therefore, slight errors in the absolute magnitude are not significant.

In some cases during testing, the quality of the received signal degraded with time. This is probably due to slow diffusion of water through the epoxy. In these cases, determination of the location of the first arrival was difficult, and required judgement. To aid in this, a digital filter was occasionally used to filter high and low frequency electrical noise. Based on an approach used by Filz (1992), the signals were filtered using the program MathCAD. An example of the MathCAD file used to digitally filter the received signals is shown in Appendix A.

4.4.2 Electrical Conductivity of Sands

For a given resistance to the flow of electrons (R), there is a direct relationship between the voltage (V) and the current (I) through a medium. This can be written as

$$V = IR \tag{4.2}$$

The units for these terms are volts, amps, and ohms, respectively. This well known relationship is called Ohm's Law, and is analogous to other one dimensional direct flow relationships, such as Darcy's Law for the flow of water and Fick's Law for the flow of chemicals (Mitchell 1993).

The resistance is a function of the medium and is dependent on both the length of the medium and the cross-sectional area through which the electrons flow. The effects of the length and area can be removed by rewriting the resistance as

$$\rho = \frac{RA}{L} \tag{4.3}$$

where

L = length, m

A = cross sectional area, m^2

ρ = electical resistivity, ohm-m^2

If the resistivity represents the relative difficulty of electron flow, its reciprocal represents the relative ease with which current can pass through a medium. This can be written as

$$\sigma = \frac{1}{\rho} = \frac{1}{R}\frac{L}{A} \tag{4.4}$$

where

σ = electrical conductivity, with units of 1/ohm m^2 = mho/m^2 = siemens/m^2

For soil-water systems the electrical conductivity is a function of the pore fluid composition, porosity, degree of saturation, surface conductance of the particles, the shape and orientation of the particles, temperature, and pressure (Sadek 1993). The flow of electrons can only travel three ways in such systems: through the pore fluid, directly

through the particles, or along the surface of the particles. Only in clays is there enough surface conductance, due to the diffuse double layer, for significant flow to occur along the surface of the particles. Also, the electrical resistance of the soil particles to current is quite high. Therefore, this path of current does not occur in sands, and the flow of electrons occurs entirely through the pore fluid in the voids of the specimen.

4.4.2.1 Influence of Pore Fluid Conductivity on Electrical Conductivity

Because the flow of electrons in a saturated sand sample is almost entirely through the pore fluid, the measured electrical conductivity of the soil-water system is heavily dependent on the conductivity of the pore fluid. The pore fluid conductivity is itself dependent on a number of factors, including the amount of ions in solution and the temperature. Figure 4.21 shows how an increase in the concentration of sodium chloride in solution affects the measured water conductivity.

Experiments on clean sands have shown that the conductivity of the soil-water system is directly related to the pore fluid conductivity (Archie 1942), and can be written as

$$\sigma_w = F\sigma_s$$

or

$$F = \frac{\sigma_w}{\sigma_s} \tag{4.5}$$

where

σ_w = the electrical conductivity of the pore fluid

σ_s = the electrical conductivity of the soil-water system

F = a formation factor

The formation factor reflects the actual path that current must flow through the soil, and is solely a function of the pore space and fabric of the sand skeleton.

4.4.2.2 Influence of Soil Fabric on Electrical Conductivity

Soil fabric is an important aspect of the measured electrical conductivity. If a sample is anisotropic, the conductivity will be different depending on the direction. Measuring the soil-water conductivity in the horizontal and vertical directions for such a sample will yield different formation factors, F_h and F_v. Arulanandan and Kutter (1978) presented a parameter to account for potential anisotropy in electrical conductivity measurements, which is shown below.

$$A = \sqrt{\frac{F_v}{F_h}} \tag{4.6}$$

where

A = the anisotropy index

Substituting equation 4.5 for the vertical and horizontal formation factors, the anisotropy index can be directly determined from the soil-water conductivity as:

$$A = \sqrt{\frac{\sigma_{s,h}}{\sigma_{s,v}}} \tag{4.7}$$

This shows that an increase in anisotropy index would indicate the development of a more horizontally aligned fabric.

Arulanandan and Kutter presented conductivity data for two different sands, which is shown in Table 4.3.

Table 4.3 Electrical conductivity data for two sands
(Arulanandan and Kutter 1978).

	F_v	F_h	A	n
Monterey 0 sand (pluviated)	4.05	3.91	1.016	0.38
Ottawa sand (pluviated)	4.05	3.99	1.006	0.361

Human (1992) obtained values of A of 1.01 to 1.25 for samples of Crystal silica sand in rigid wall cells for vertical stresses of 50 and 150 kPa, respectively.

4.4.2.3 Influence of Cementation on Electrical Conductivity

Archie (1942) reported that the formation factor was related to the porosity as follows:

$$F = n^{-m} \tag{4.8}$$

where

n = porosity

m = slope of the log formation factor – log porosity relationship

Values of m for consolidated sandstones ranged between 1.8 and 2.0, and for clean sands in the laboratory m was equal to 1.3. Thus, for the same porosity, the sandstone yields a higher formation factor. This suggests that cementation decreases σ_s and thus restricts current flow through the pore spaces.

Wyllie and Gregory (1953) studied the effect of artificial cementation, using silica, on the measured formation factor. They proposed that Equation 3.2 was simply a special case of the more general relationship

$$F = C\,n^{-k} \tag{4.9}$$

where C depends on the porosity and formation factor prior to cementation and k depends on the type of cement used. For their experiments, k was found to be 4.2.

4.4.2.4 Motivation for Measuring Electrical Conductivity during Aging

Electrical conductivity measurements were chosen for this study for three reasons. First, these measurements are thought to be non-destructive and therefore can be performed throughout the aging process. Monitoring the pore fluid conductivity with time has the added benefit that the dissolution and possible precipitation of minerals can be observed.

An increase in the pore fluid conductivity indicates that dissolution is occurring while a decrease would indicate that ions are being removed from solution, possibly due to precipitation. The third reason is that, by measuring the conductivity of the soil-water system in two different directions (horizontal and vertical), one can look for changes in fabric that might be indicative of small particle rearrangements.

4.4.2.5 Equipment Details

The most basic way to measure electrical conductivity in the laboratory is shown in Figure 4.22 (a). In this case the electrodes cover the ends of the specimen and the flow of electrons is entirely one dimensional. Here, Ohm's Law can be applied directly to measure the sample resistance, and the corresponding conductivity. To measure the conductivity in more than one direction, however, this setup does not work. Electricity will follow the path of least resistance, and for electrodes that cover the entire base or side of a cell, the current from a vertical electrode would short circuit to one of the horizontal electrodes and vice versa. The consequence of this is that, in order to measure conductivity in the horizontal and vertical directions, smaller electrodes must be used. The size of the electrodes must be such that the distance between any vertical and horizontal electrode must be greater than half the distance between electrodes of the same type.

The electrodes used for this study are shown in Figure 4.22 (b) and their placement in the rigid wall cells is shown in Figure 4.1. The electrodes were constructed of stainless steel foil and were glued to the cells using Scotchweld Brand DP-190 epoxy manufactured by 3M. The outer electrodes are used to generate the current, while the inner electrodes are used to measure the corresponding voltage drop. This setup is similar to that used by Human (1992). With this setup, the soil-water conductivity can be measured in both the horizontal and vertical directions.

4.4.2.6 Determination of Cell Constants

Using electrodes that do not cover the full width of a specimen results in a flow of electrons that is no longer one dimensional, as shown in Figure 4.22 (b). For these conditions, Equation 4.4 no longer strictly applies. The two dimensional flow conditions are due to the geometry of the electrodes and can be accounted for with the introduction of a shape factor, SF, as shown below.

$$\sigma = \frac{1}{R}\frac{L}{A}SF = \frac{1}{R}K \tag{4.10}$$

For a given placement of electrodes, the terms (L/A)SF can be lumped together into a cell constant, K, which can then be determined experimentally. If water of a known conductivity is placed in the cell, the cell constant can be determined by rearranging Equation 4.10 as

$$K = \sigma_w R \tag{4.11}$$

The resistance R is determined by applying a current across the current electrodes, measuring the corresponding voltage drop, and using Ohm's Law to determine R. Figure 4.23 shows how the cell constants were determined for one of the eight cells. The cell constants were determined for both the vertical and horizontal electrodes, and were calculated using the measured pore water conductivity of a sodium chloride solution.

Electrical conductivity is heavily dependent on temperature because of increased ion mobility in the solution, and small increases in temperature can cause large increases in the measured conductivity. Because of this, it was important to know how temperature affected the cell constant, K. Figure 4.24 shows the measured vertical and horizontal cell constants as a function of temperature. Two things are apparent from the results: the cell constants are independent of temperature and the four cells tested had approximately the

same cell constants. Because the geometries of the electrodes were identical for the eight cells, a vertical cell constant of $K_v = 0.235$ and a horizontal cell constant of $K_h = 0.177$ was used for all cells.

4.4.2.7 Measuring Soil-Water Conductivity

When measuring electrical conductivity, either direct current (DC) or alternating current (AC) can be used. Direct current causes certain coupled flow problems like electro-osmosis and ion migration, which can change the properties of the sample. With alternating current, however, the measured conductivity is frequency dependent. However, for low frequencies AC (< 100 Hz), the measured conductivity doesn't change very much and values of conductivity obtained using 60 Hz alternating current have been found to be close to values obtained using direct current (Sadek 1993). Therefore, 60 Hz alternating current was used for all the soil-water conductivity measurements.

A schematic of the measurement system is shown in Figure 4.25, where the sample acts as a simple resistor. The apparatus used to measure the soil-water conductivity included a function generator (BK Precision 3011B), and two multimeters (RSR 905 and Tenma 72-6000) to measure the alternating current and the corresponding voltage drop. A 60 Hz sine wave was applied to the current electrodes and the amplitude was increased until a given voltage was measured. The corresponding current was recorded and the amplitude was then increased until a new voltage was reached. Current readings were usually taken at 1, 2, 3, 4, and 5 volts. From Ohm's Law, the resistance (in ohms) was then calculated and the soil-water conductivity was calculated using Equation 4.10.

4.4.2.8 Measuring Pore Fluid Conductivity

The pore fluid conductivity in the samples was measured with a conductivity meter on approximately 40 ml of fluid withdrawn from the drainage port in the base of each cell. Two different conductivity meters were used during the course of this study: a Barnstead

Conductivity Bridge Model PM-70 CB and an Acumet AB30 conductivity meter. The Acumet AB30 was much easier to operate and was used for the majority of the tests.

Because of the temperature dependence of electrical conductivity, the pore fluid samples were always in water baths to maintain a constant temperature while the pore fluid conductivity measurements were taken. For each reading, usually two or three samples of 40 ml volume were taken, and an average conductivity reading was used. After measuring the pore fluid conductivity, the pore fluid samples were put back into the cell through the drainage port.

4.4.3 Mini-Cone Penetration Tests

4.4.3.1 Motivation for Performing Mini-Cone Penetration Tests during Aging

Unlike the previous two test methods, penetration tests using a mini-cone are destructive and can only be performed once on a given sample. However, there are advantages to performing this type of test to assess aging effects in sands. Cone penetration tests are the most common method used for investigating aging effects reported in the literature. As such it is important to be able to relate the results of any laboratory study to what is occurring in the field. In this way, the results of this study are of more practical interest to engineers.

Unlike the small strain shear modulus tests, cone penetration tests measure soil properties at large strains. However, the measured penetration resistance depends on small strain properties as well as large strain properties because the penetrometer zone of influence extends a significant distance (many diameters) from the cone. A testing program using penetration tests in conjunction with small strain shear modulus measurements provides information on aging effects for both small and large strain conditions.

4.4.3.2 Equipment Details

A schematic of the mini-cone penetration test setup is shown in Figure 4.26. A simple system was constructed involving a 0.635 cm diameter steel probe (mini-cone) with a 60^{o} apex angle at one end. This probe is not instrumented like a traditional cone; it is simply connected to a 500 pound load cell (Omega LCC). The output from the load cell was sent to a strip chart recorder, where the penetration resistance as a function of sample depth was plotted.

The mini-cone was pushed into a sample using a hydraulic piston with a maximum extension of approximately 20 cm. With the hydraulic piston, a constant push rate of 0.5 cm/sec was used for all the tests.

The piston was attached by a reaction beam to two, freestanding posts. This ensured that at no time during the penetration testing was the load frame disturbed in any way.

The mini-cone penetration tests were performed while the samples were still under load in the load frame. This was accomplished by drilling two holes in each top cap, as shown in Figure 4.1. With this setup, two penetration tests could be performed on a single sample. The location of the holes was governed by the geometry of the load frame and the lever arms acting on the samples.

Ideally, the penetration test should be done in the center of the sample. This would minimize the effect of the rigid boundary wall on the penetration resistance. In order to simulate free-field conditions, where the boundary would have no influence on the penetration resistance, the ratio of cell diameter to cone diameter should be greater than 20 for loose sands and greater than 50 for dense sands (Lunne et al. 1997). The mini-cone penetration tests in this study were performed only 3 cm from cell wall; clearly the results are not free-field measurements. However, the penetration resistance can still measure changes in the penetration resistance due to aging since the boundary effect will

be the same throughout the test. Mini-cone penetration tests were performed at the end of a period of aging, and the results were compared to the results of tests performed on identically prepared samples with no period of aging. The second hole in the top cap was used for duplicate tests to assess the variability in the sample caused by sample preparation and to look for possible sensitivity caused by the first penetration test.

4.5 Laboratory Testing Program

The laboratory testing program performed in this study focused primarily on testing the possible mechanical and chemical hypotheses that might be responsible for aging effects in sands. Aspects of the blast gas dissipation hypothesis were also investigated, but there was no focus on biological activity or possible pressure solution in the tests.

4.5.1 Variables Tested

The approach of this study for gaining insight into the mechanisms responsible for aging is to study the influence of different variables on the presence and magnitude of aging effects. The variables chosen for this study were sand type, vertical stress, temperature, relative density, and pore fluid composition. The values of each variable that were tested are shown in Table 4.4 for both the rigid wall tests and the bucket tests, and each variable is described in more detail below.

Table 4.4 Variables tested in this laboratory study.

RIGID WALL TESTS

Sand Type	Vertical Stress	Temperature	Relative Density	Pore Fluid Composition
Evanston sand Density sand	100 kPa	20^{o} C 40^{o} C	40% 80%	Distilled water Ethylene Glycol CO_2 saturated water Air (dry)

BUCKET TESTS

Sand Type	Vertical Stress	Temperature	Relative Density	Pore Fluid Composition
Evanston sand Lightcastle sand	~0 kPa	~20^{o} C	~60%	Distilled water 0.1 M NaCl

4.5.1.1 Sand Type

The properties of the three sands tested are presented in section 4.3. Evanston sand was chosen because Dowding and Hryciw (1986) observed increases in penetration resistance following blasting in a laboratory study using this sand. It was important to use a sand in this study where aging effects were known to have already occurred. Density sand was chosen because it is a pure quartz sand, which would narrow the potential chemical hypotheses to dissolution/precipitation reactions involving silica. Lightcastle sand was used only for the bucket tests. It is a quartz sand and was chosen because it was readily available in large quantities.

4.5.1.2 Vertical Stress

All of the rigid wall tests were performed at a vertical stress of 100 kPa. Examples of aging effects have been cited for a wide range of stress levels ranging from near zero (Dowding and Hryciw 1986) to approximately 600 kPa (Mitchell and Solymar 1984), and 100 kPa is a reasonable median value. This would correspond to a depth of 10 m for a soil with a buoyant unit weight of 10 kN/m^3 and the groundwater table at the surface. The bucket tests, however, were aged with no surcharge. Thus the stresses present in the bucket tests were very low, and were due only to the buoyant weight of the sand.

4.5.1.3 Temperature

The rigid wall tests were performed at either 25^o C or 40^o C. The temperature was held constant by immersing the cells in heated water baths. As discussed in section 3.4.2, the solubility of silica increases with temperature (a 30% increase from 25^o C to 50^o C), while the solubility of calcite decreases slightly with increasing temperature. Thus, by increasing the temperature, one can focus on the hypothesis involving the dissolution and precipitation of amorphous silica as a possible mechanism for aging effects.

The bucket tests were performed at room temperature, and the temperature in the samples ranged from 17.4^{o} C to 23.7^{o} C over a period of approximately 100 days.

4.5.1.4 Relative Density

Samples in the rigid wall cells were prepared to either 40% or 80% relative density. These two conditions were chosen because it is not known whether the aging phenomenon is more significant for loose or dense sands. Most examples of aging effects involve the densification of loose sands to a denser condition. The sand in the buckets were prepared to an approximate relative density of 70%.

4.4.1.5 Pore Fluid Composition

Four different pore fluids were used in this study: distilled water, ethylene glycol, distilled water saturated with carbon dioxide, and a 0.1 molar sodium chloride solution. Dry samples were also tested. The distilled water was chosen as a baseline pore fluid so that the results of the other tests could be compared to it. Distilled water is not representative of natural groundwater conditions, but with it there is less uncertainty about biological activity and the chemical constituents of the water.

Ethylene glycol was chosen specifically to investigate possible mechanical mechanisms. Unlike water, the solubility of both silica and calcium carbonate in ethylene glycol is negligible. Thus, if a chemical mechanism is responsible for aging effects in sands, it should not occur with ethylene glycol as a pore fluid.

Likewise, it is not expected that dissolution/precipitation reactions would occur in dry sands. Thus, two samples in rigid wall cells were tested dry, with no pore fluid. These tests were performed at room temperature only, because it was not possible to keep the dry samples at 40^{o} C.

As discussed in section 3.5.2 regarding the blast gas dissipation hypothesis, the dissolution of carbon dioxide gas in water results in the formation of carbonic acid, which decreases the pH of the water. As the pH decreases, the solubility of carbonate minerals increases dramatically while the solubility of silica remains unchanged. Therefore, using water saturated with carbon dioxide specifically targets the hypothesis that the dissolution and precipitation of carbonate minerals contributes to aging effects.

Just prior to pouring the sand into the pore fluid, water was saturated with carbon dioxide by bubbling the gas through the water for approximately 10 minutes, while monitoring the pH. This caused a change in the pH from approximately 7 to 3. For 1 atm total pressure, a pH of 3 corresponds to carbon dioxide saturation in water.

For some of the bucket tests, a 0.1 molar sodium chloride solution was used as a pore fluid. This corresponds to 5.84 grams of sodium chloride per liter of solution. This was chosen to investigate if, in contrast to distilled water, the presence of ions in solution would affect the presence or magnitude of aging effects.

4.5.2 Sample Preparation

This section describes the sample preparation for the rigid wall tests only; the bucket tests are described in section 4.5.5. One to two weeks prior to forming the samples, a known weight of air-dried sand was placed in buckets and immersed in the pore fluid for the test. This was done in an effort to approach an equilibrium condition between the sand and the pore fluid prior to aging. This is more representative of saturated sands in nature, which are in equilibrium with the groundwater long before ground modification or in situ testing is performed. Because of the way the load frames were constructed, the samples needed to be approximately 16.2 cm in height. Therefore, a known dry weight of sand was prepared such that at a height of 16.2 cm, the sample would be at the desired relative density.

In order to ensure that the samples were fully saturated, the samples were formed by pluviating the sand through the pore fluid, in a method similar to that proposed by Bishop and Henkel (1957). The cells were first filled with the pore fluid and, using a funnel, sand and fluid was pluviated into the cell. As the sample was formed, the fluid level rose and eventually over-topped the cell. Care was taken not to lose any of the sand during pluviation. To prevent scour of the sample due to the pluviation, a temporary 7.5 cm piece of PVC pipe was glued to the cell wall to extend the length of pluviation. This is shown in Figure 4.28. With this procedure, uniform loose samples were fabricated. The relative densities immediately after pluviation ranged from 30 to 35%.

After pluviation, the extenders were removed and the cells were carefully moved onto a vibrating table in order to densify the loose specimens to the proper height, and thus the desired relative density. The samples were vibrated without a surcharge or the top caps. The samples prepared to a relative density of 40% required very little vibration, whereas the samples prepared to 80% relative density required repeated periods of vibration, followed each time by a check of the sand height. This method of achieving either a loose or a dense sample was chosen to very loosely simulate ground improvement. Although this method is clearly different than techniques like blast densification, densification of the samples was caused by energy imparted to the soil through horizontal vibration.

When the desired density was achieved, the cells were very carefully transferred to the load frame. The top cap was then placed on the sand, taking care to line up the transmitting and the receiving bender element in the same plane. Once the top cap was in place, the initial height of the sample was recorded, and the acrylic settlement post, the linear motion bearing, and the ball bearing were all assembled. Before placing the lever arm on the sample (which served as a seating load) and attaching a dial gauge, a circle of plastic wrap was placed over the sample to prevent contamination and evaporation of the pore fluid during the test.

After the seating load was applied, the temperature in the water bath was raised to either 25^{o} C or 40^{o} C. In this way, any expansion of the composite cell walls due to temperature change occurred prior to full loading to 100kPa.

For the samples that were tested dry, dry pluviation was used to form the samples. The sand was pluviated from a bottle with a single hole sized specifically to achieve a relative density of 80%. The sand fell from the hole a constant height of 25 cm above the surface of the sand.

All the samples were loaded in three or four increments up to a final vertical stress of 100 kPa. After each load increment, the settlement and shear wave velocity were measured. The start of the aging process was considered to be the moment the vertical stress was increased to 100 kPa.

4.5.3 Schedule of Rigid Wall Tests

Twenty two rigid wall tests were performed for this study. The specific variable levels for each test are listed in Table 4.5. The results of these tests are presented in chapter 5.

Table 4.5 Schedule of rigid wall tests performed in this study.

Test No.	Sand Type	Vertical Stress (kPa)	Temperature (^{o} C)	Relative Density (%)	Pore Fluid	Period of Aging (days)
1	Evanston	100	25	40	distilled water	40
2	Evanston	100	25	40	ethylene glycol	40
3	Evanston	100	25	40	CO_2 - water	37
4	Evanston	100	25	80	distilled water	40
5	Evanston	100	25	80	ethylene glycol	40
6	Evanston	100	25	80	CO_2 - water	36
7	Evanston	100	~22	80	dry	48
8	Evanston	100	40	40	distilled water	30
9	Evanston	100	40	40	ethylene glycol	30
10	Evanston	100	40	80	distilled water	118
11	Evanston	100	40	80	ethylene glycol	106
12	Density	100	25	40	distilled water	40
13	Density	100	25	40	ethylene glycol	40
14	Density	100	25	40	CO_2 - water	33
15	Density	100	25	80	distilled water	40
16	Density	100	25	80	ethylene glycol	40
17	Density	100	25	80	CO_2 - water	33
18	Density	100	~22	80	dry	48
19	Density	100	40	40	distilled water	31
20	Density	100	40	40	ethylene glycol	30
21	Density	100	40	80	distilled water	118
22	Density	100	40	80	ethylene glycol	106

4.5.4 Mineralogical Tests

In conjunction with the above testing program, detailed mineralogical studies of the sand and pore fluid before and after aging were performed. These included the following:

- Inductively Coupled Plasma (ICP) analyses for determining the chemical composition of the pore fluid after aging. This was useful in determining what elements had dissolved into solution throughout the tests.
- Carbonate Titration for determining the amount of calcium carbonate that dissolved into solution during the aging process.

- Bulk chemistry of Evanston and Density sand. The results of these tests are presented in section 4.3 and show the chemical composition of both sands.
- Scanning Electron Microscopy (SEM) was used to look for visual evidence of precipitation on and in between sand grains after aging.
- Energy Dispersive Spectrum (EDS) analysis was used as part of the SEM to determine the chemical composition of individual sand grains and possible precipitation.

For the ICP and the carbonate titration tests, samples of pore fluid were withdrawn from the drainage port of the samples at the conclusion of each test. The ethylene glycol could not be tested for dissolved material, but it is unlikely that any significant amount of material dissolved in the ethylene glycol.

After the tests were completed, the samples were drained and removed from the load frame. The top cap was removed, and samples of the sand were carefully removed and allowed to air-dry. These samples were then mounted on a slide and coated with carbon for use in the scanning electron microscope. Thus, the samples were not undisturbed, however, great care was taken to disturb the sand as little as possible.

4.5.5 Bucket Tests

In addition to the testing program involving the rigid wall cells, four series of mini-cone penetration tests in sand-filled buckets were performed. The purpose of these tests was to conduct simple tests to study the effect of sand type and pore fluid composition on aging effects at low effective stress conditions. Evanston and Lightcastle sands were used, and distilled water and a 0.1 molar sodium chloride solution were chosen for the pore fluids. The bucket tests were aged for up to 180 days.

The samples were prepared by pouring dry sand into a bucket filled with the pore fluid. The buckets were then shaken by hand to both densify the sand and to ensure fully saturated conditions. As a result, the relative densities of the samples ranged from approximately 65% to 75%. No surcharge was placed on the samples, so the effective stress conditions were due to the buoyant weight of the soil only.

The penetration tests were performed with the same piston and 0.635 cm diameter mini-cone used for the rigid wall tests. Because of the low stress conditions, a 100 pound load cell (Interface SSM100) was used, and the results of the penetration tests were outputted to a strip chart recorder. The push rate was 0.5 cm/sec.

In each bucket, five penetration tests were performed at different times. Figure 4.28 shows a penetration test in progress and a diagram showing the placement of each push. The temperature throughout the tests was monitored using a thermocouple installed in one of the buckets, and was found to range from 17.4^{o} C to 23.4^{o} C over approximately 100 days. Table 4.6 shows the schedule for the penetration tests that were performed.

Table 4.6 Schedule of mini-cone penetration tests for bucket tests.

Bucket No.	Sand Type	Pore Fluid	Time of Penetration Tests (days)
1	Evanston	distilled water	0, 7, 33, 100, 189
2	Lightcastle	distilled water	0, 7, 32, 99, 188
3	Evanston	0.1 M NaCl	0, 7, 30, 97, 186
4	Lightcastle	0.1 M NaCl	0, 8, 30, 97, 186

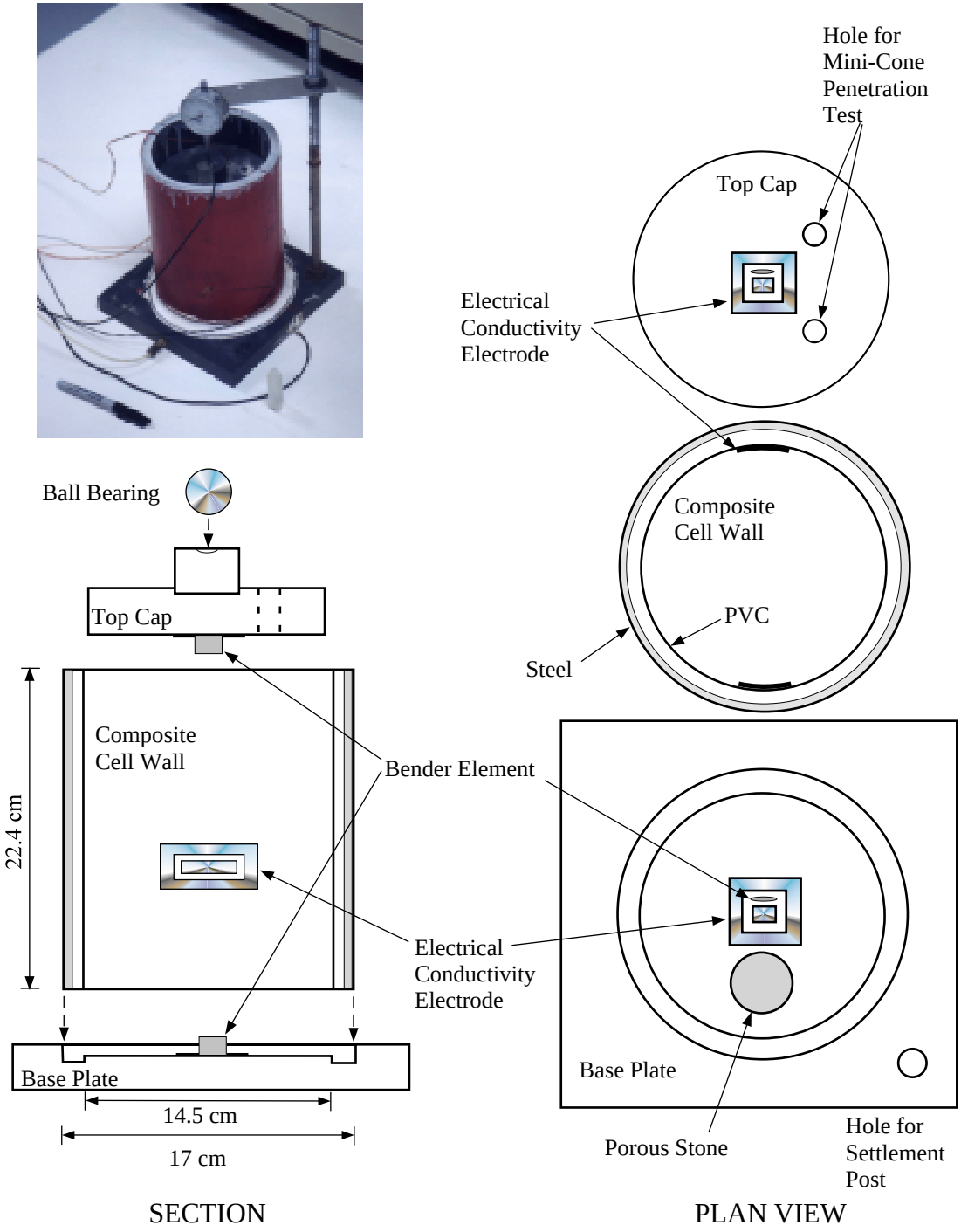

Figure 4.1 Fixed wall cell used for this study.

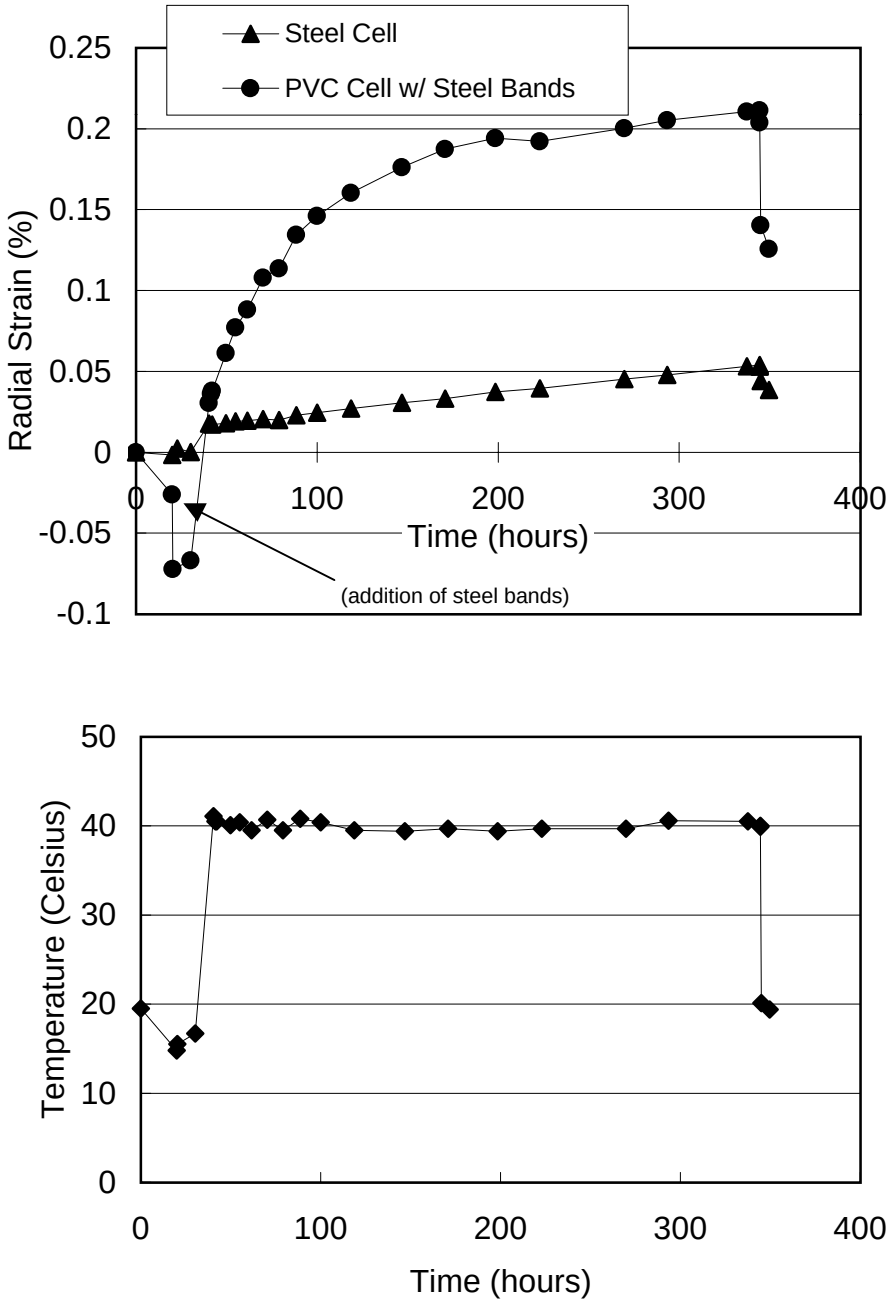

Figure 4.2 Creep of PVC and steel cell with time.

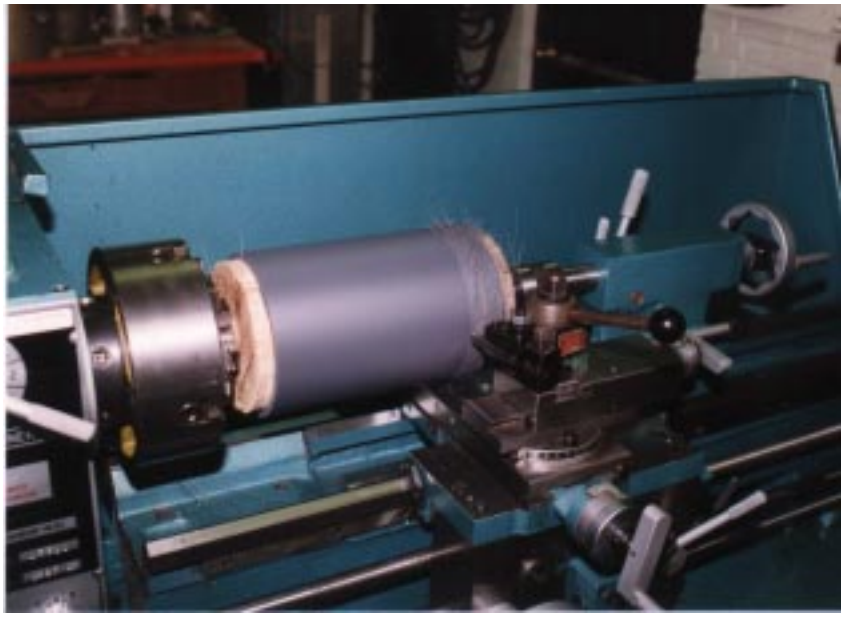

Figure 4.3 Construction of composite cell on a lathe.

Figure 4.4 Press-fitting PVC sleeve into a steel pipe.

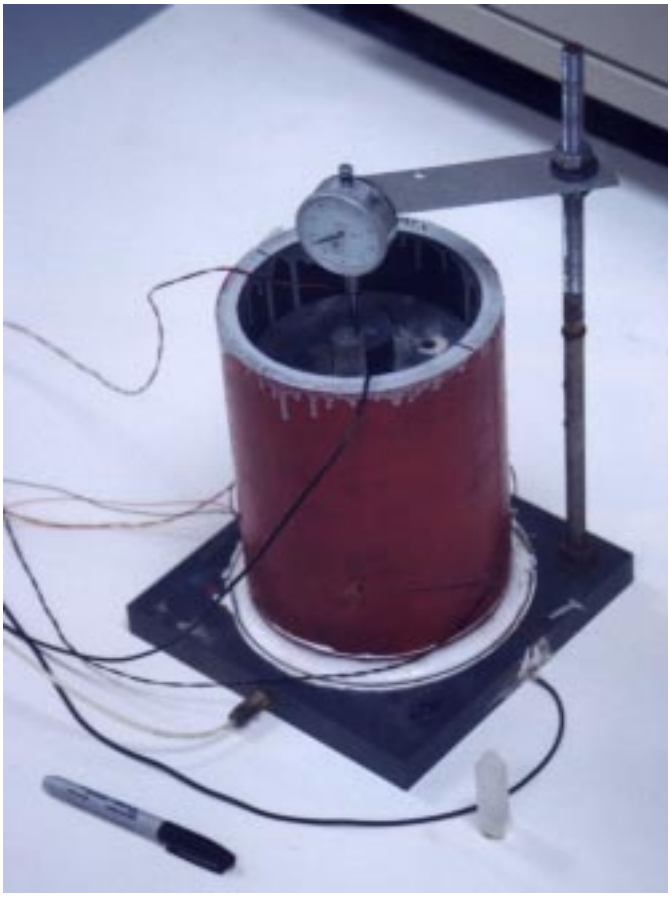

Figure 4.5 Rigid wall cell showing the dial gauge setup for measuring settlements.

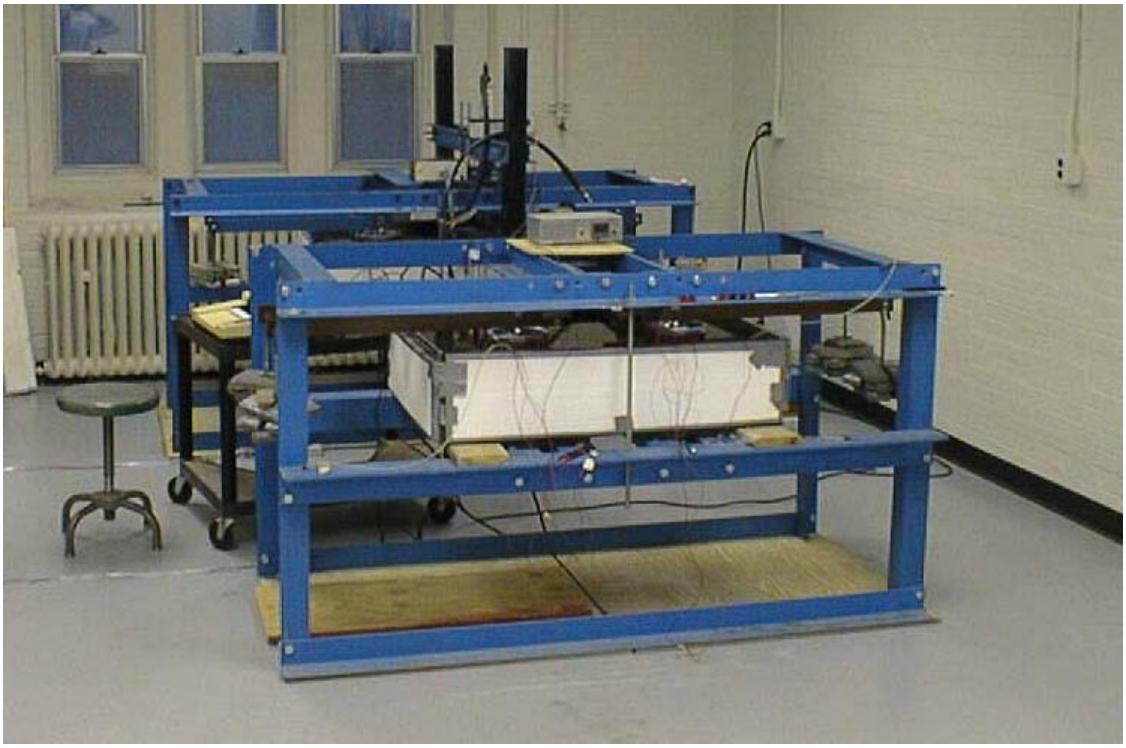

Figure 4.6 Two load frames used for this study.

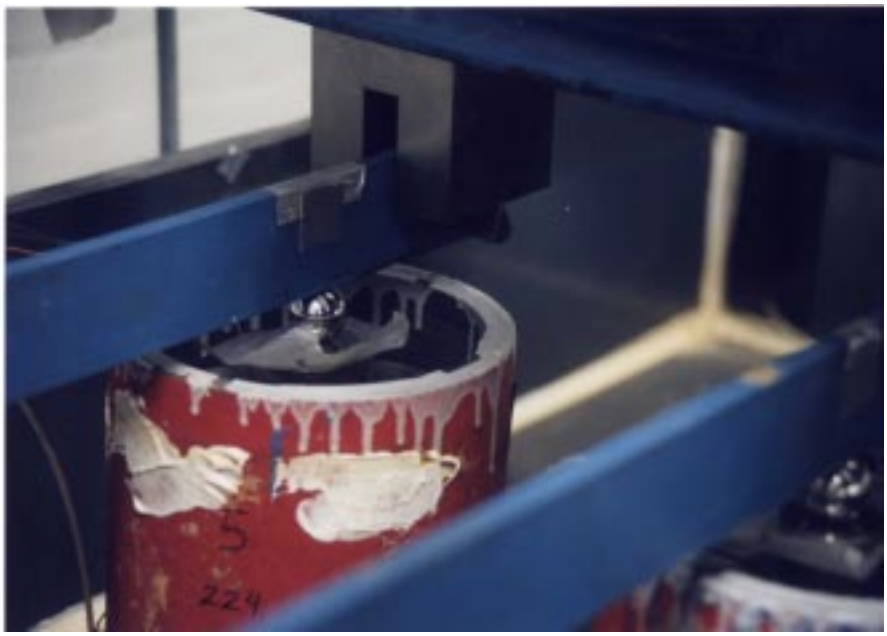

Figure 4.7 The lever arm system used to load the rigid wall cells.

Figure 4.8 Linear motion bearing.

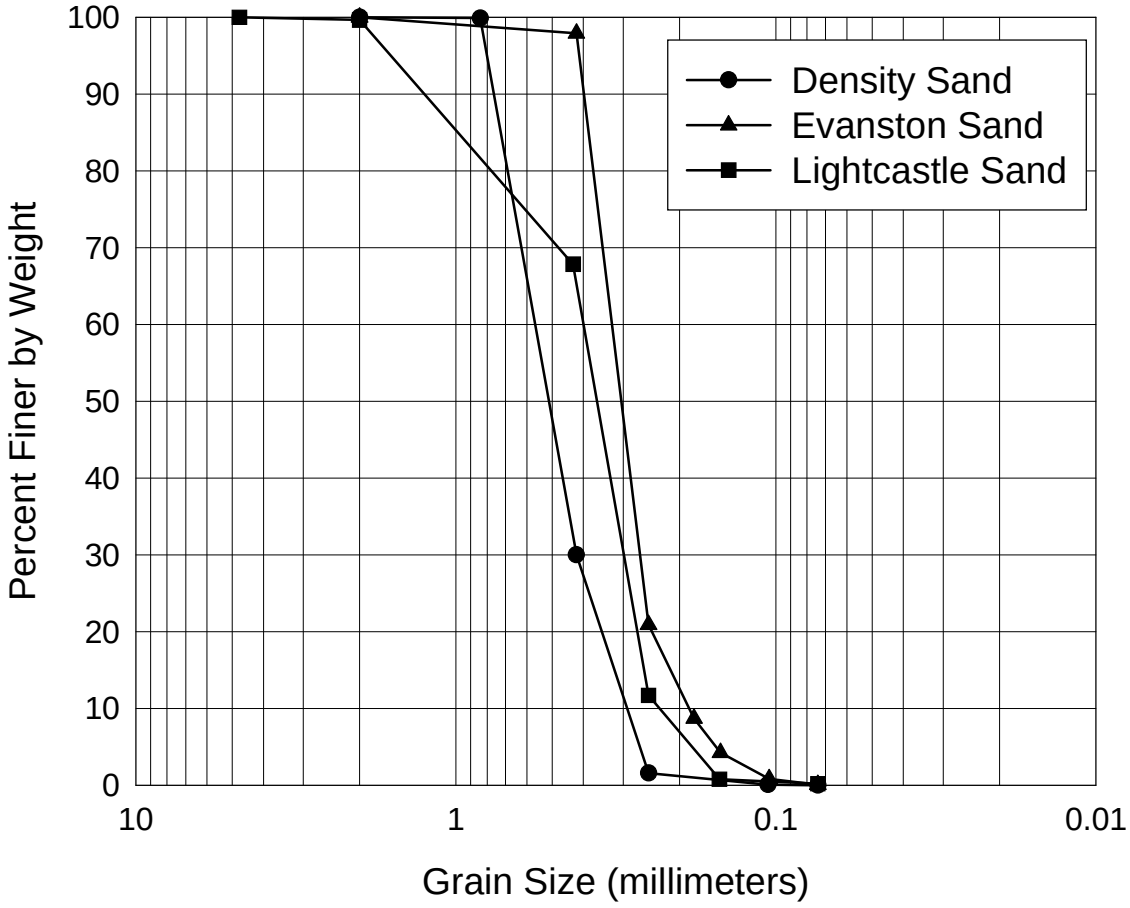

Figure 4.9 Grain size distributions for Evanston sand, Density sand, and Lightcastle sand.

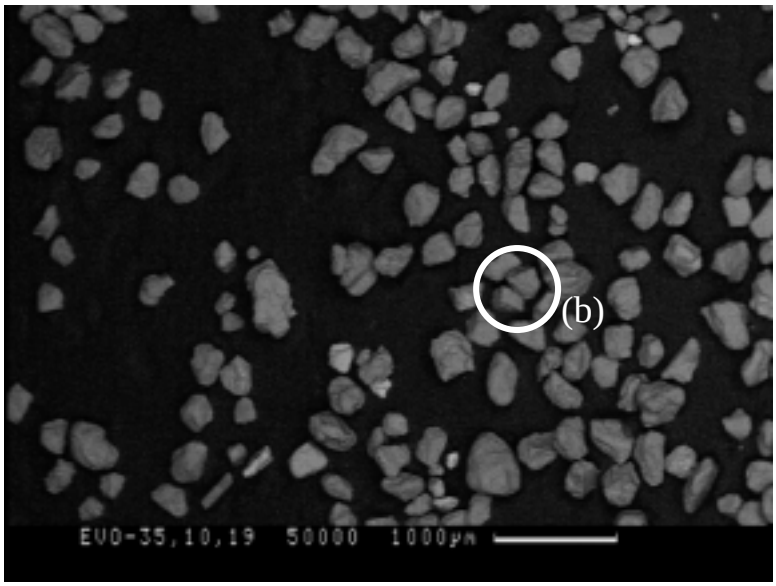

(a)

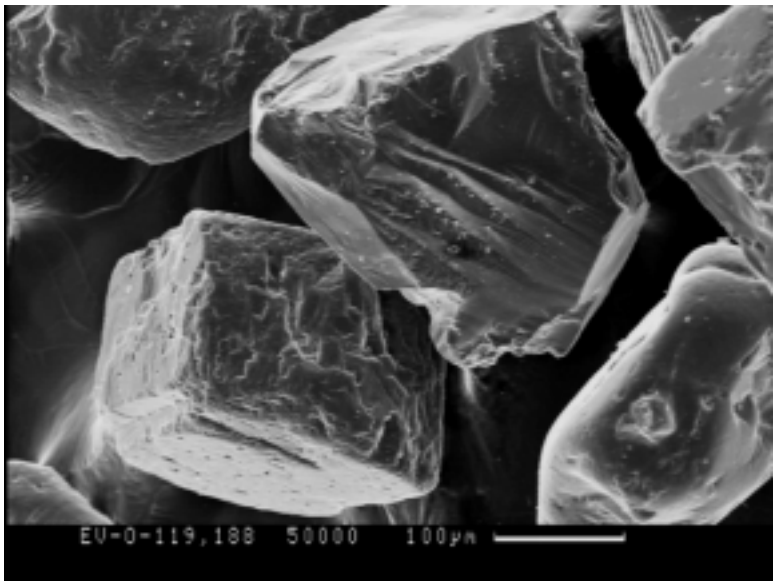

(b)

Figure 4.10 Scanning electron micrographs of Evanston sand (a) scale = 1000 μm, (b) scale = 100 μm.

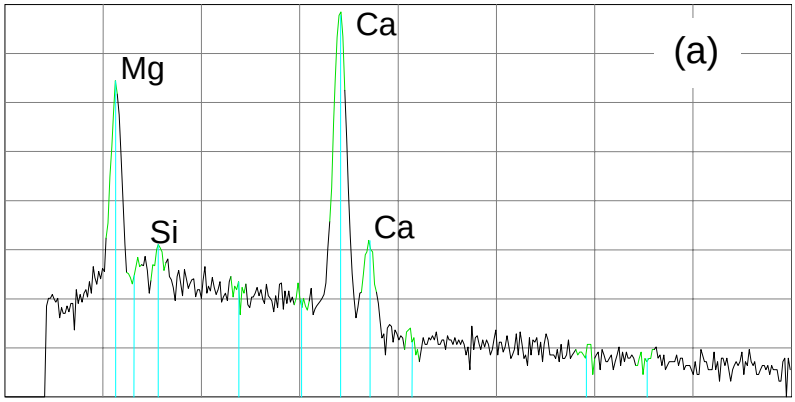

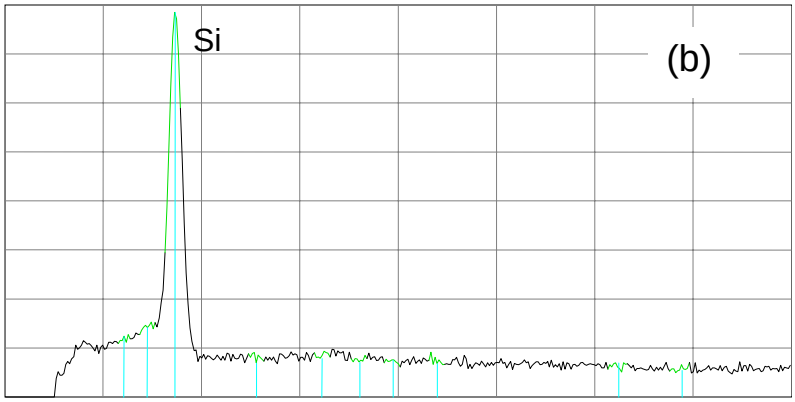

Figure 4.11 Energy dispersive spectrum for Evanston sand showing (a) dolomite, and (b) quartz

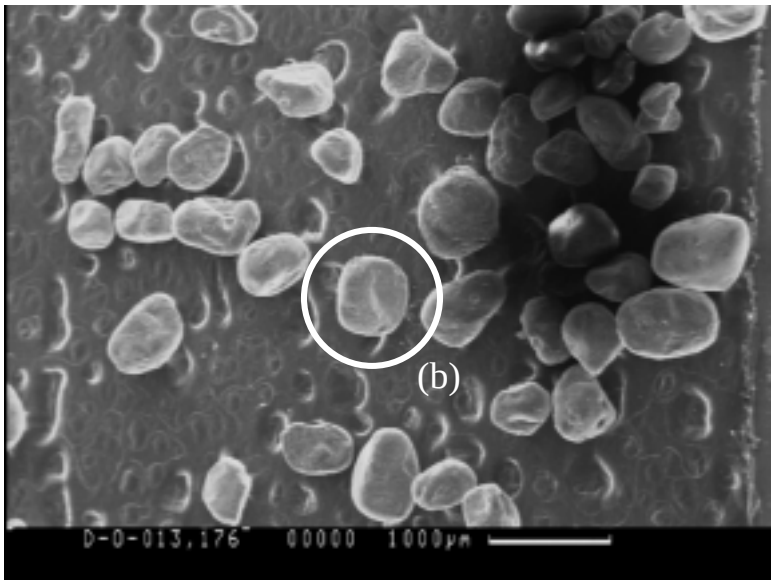

(a)

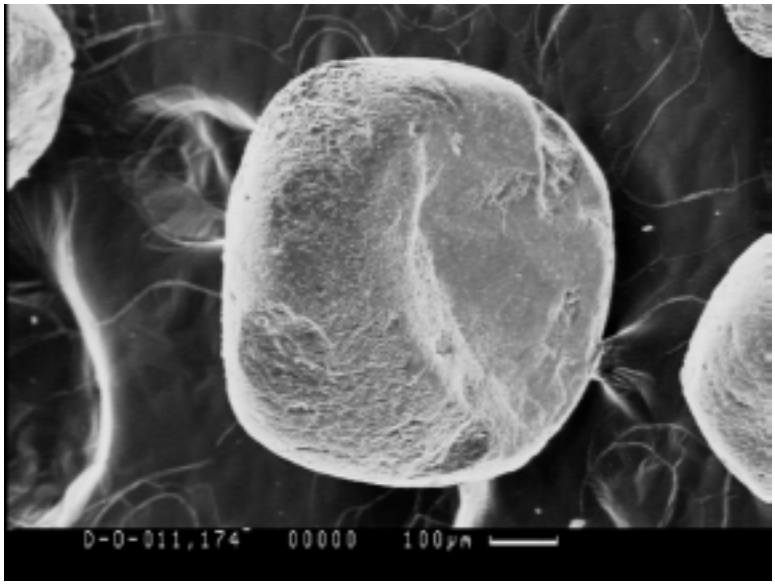

(b)

Figure 4.12 Scanning electron micrographs of Density sand (a) scale = 1000 μm, (b) scale = 100 μm.

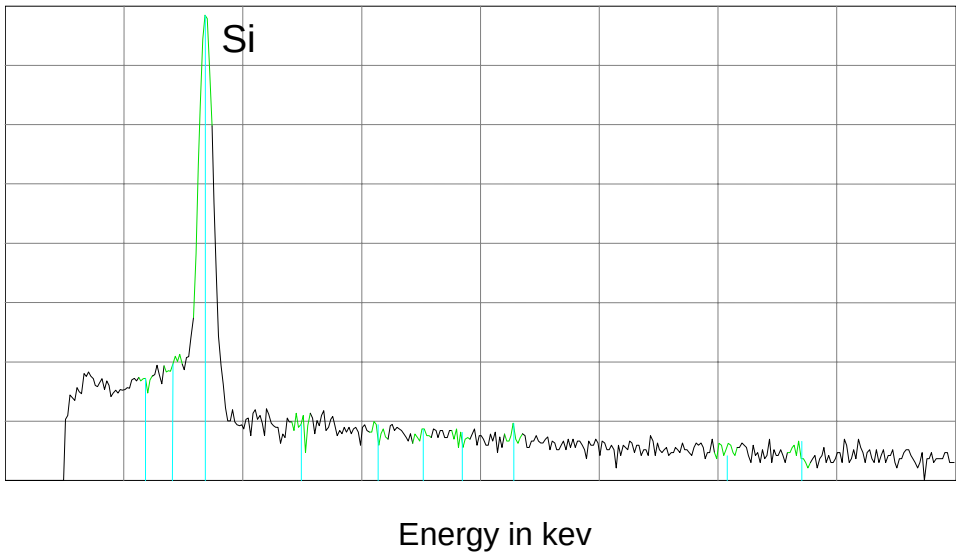

Figure 4.13 Energy dispersive spectrum of Density sand indicating quartz.

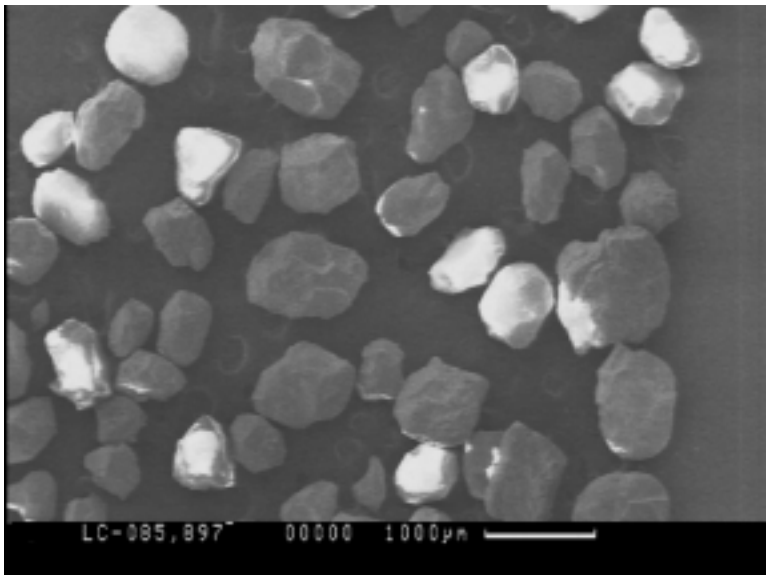

(a)

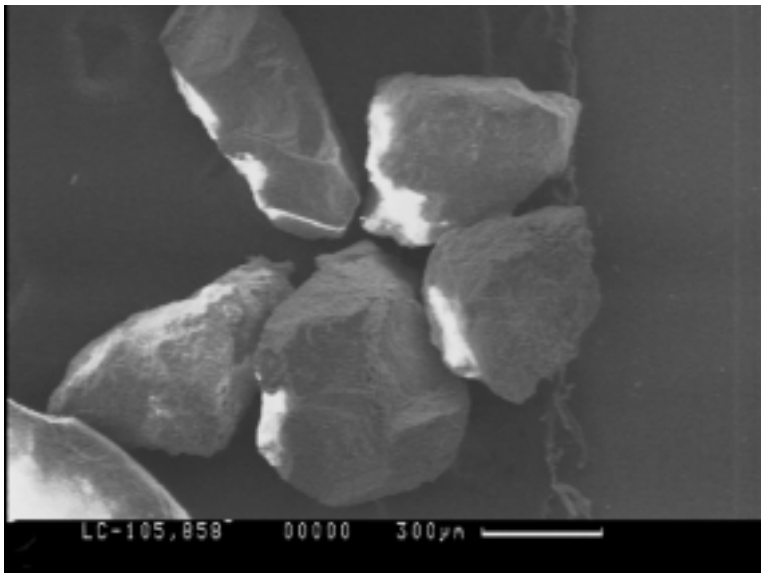

(b)

Figure 4.14 Scanning electron micrographs of Lightcastle sand (a) scale = 1000 μm, (b) scale = 100 μm.

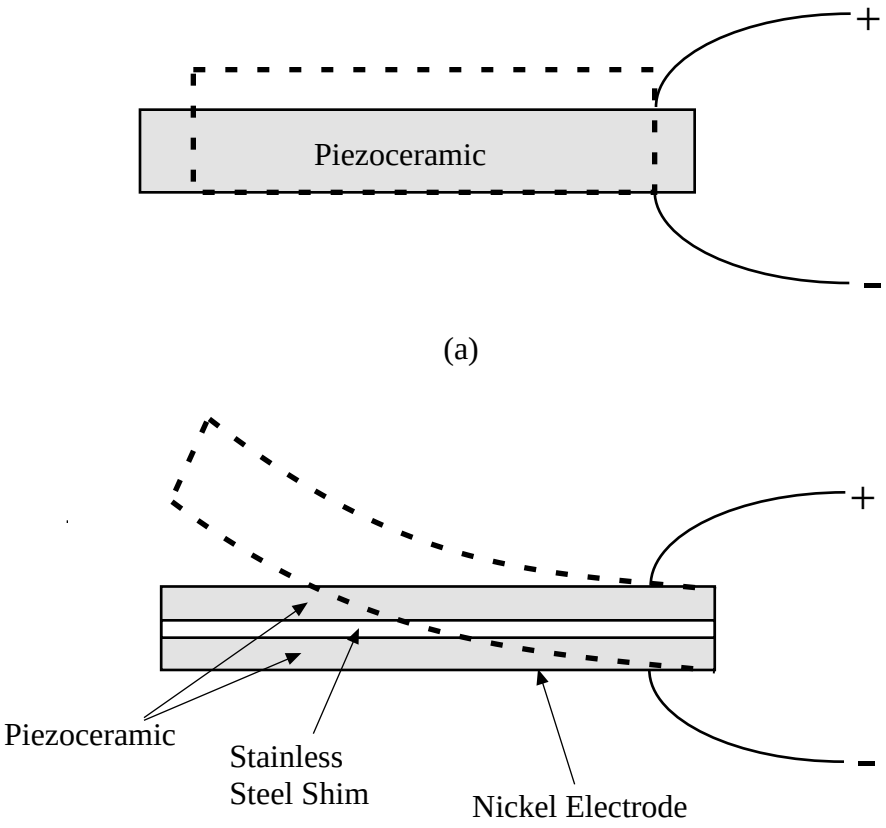

Figure 4.15 Schematic of a piezoceramic (a) single sheet and (b) double sheet "bender element".

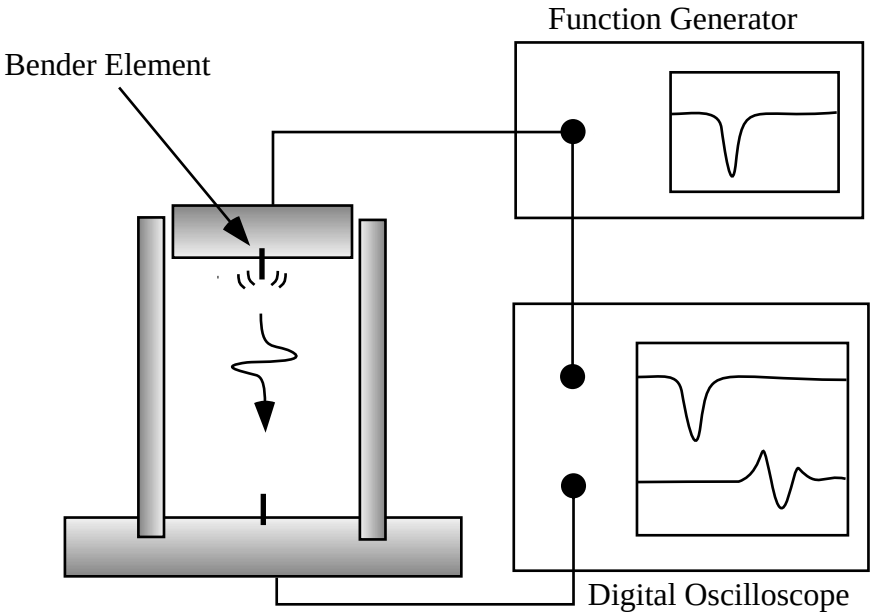

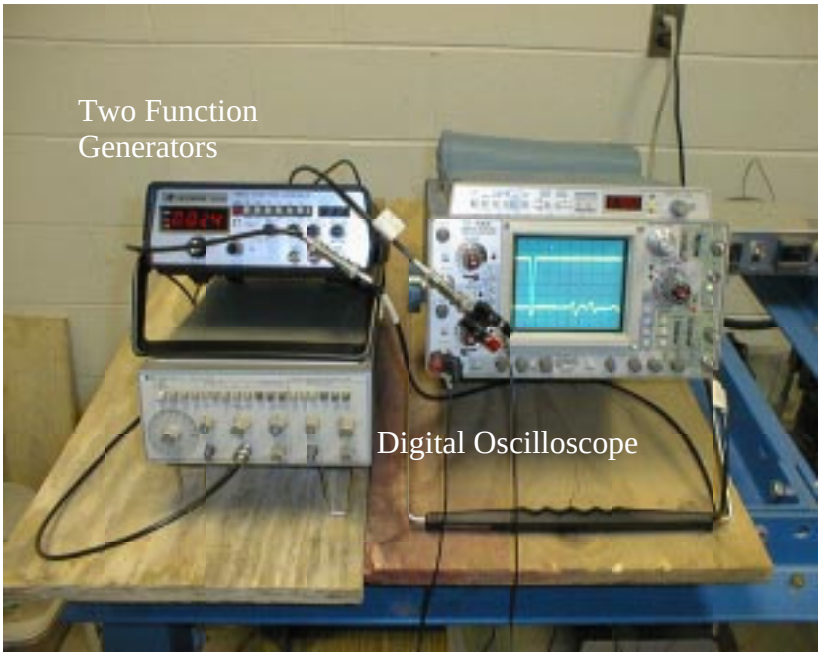

Figure 4.16 Schematic of bender element setup.

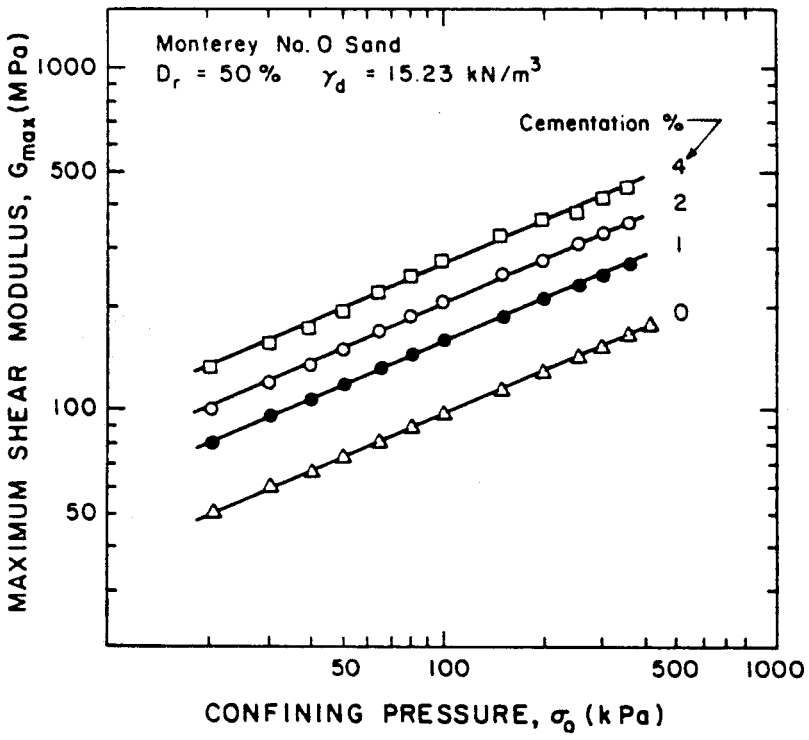

Figure 4.17 Influence of cementation on the small strain shear modulus (Acar and El-Tahir 1986).

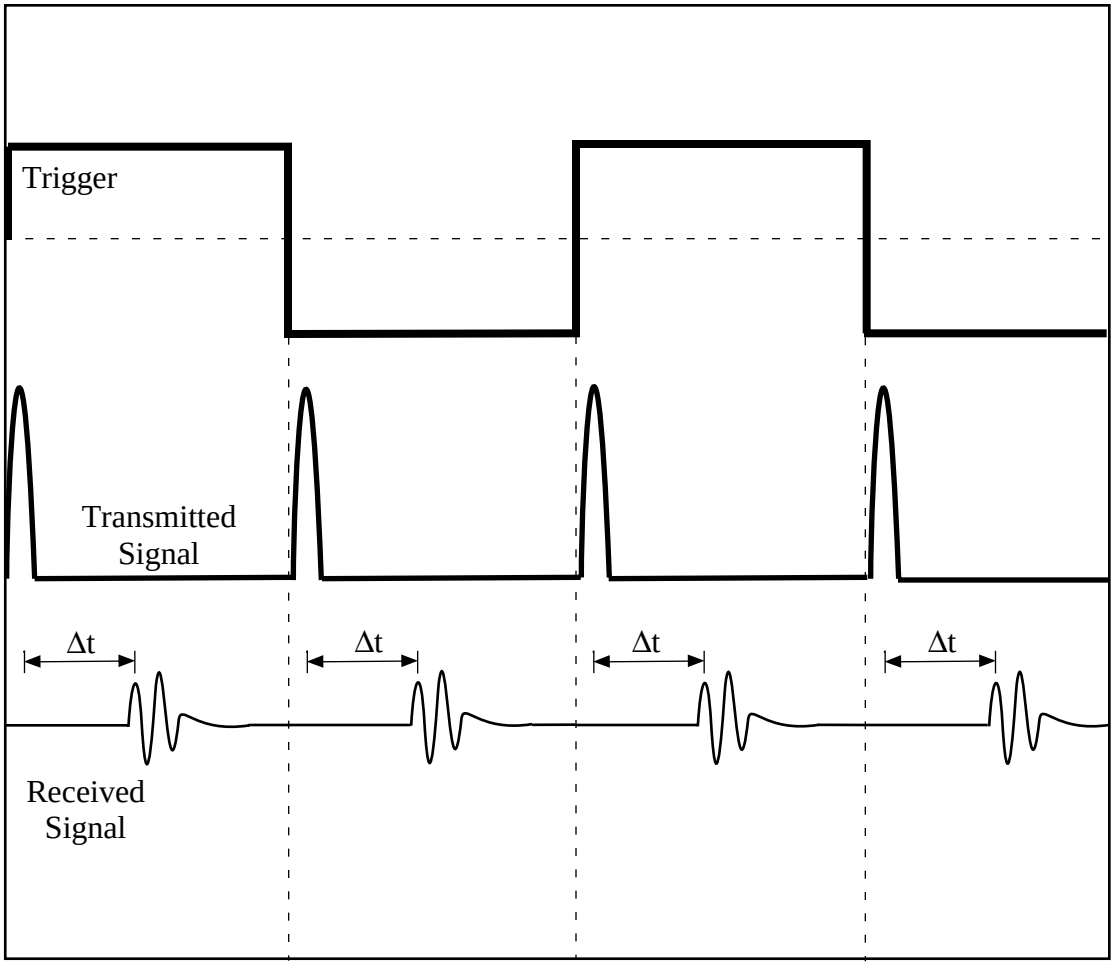

Figure 4.18 Waveforms generated by the bender element setup used in this study.

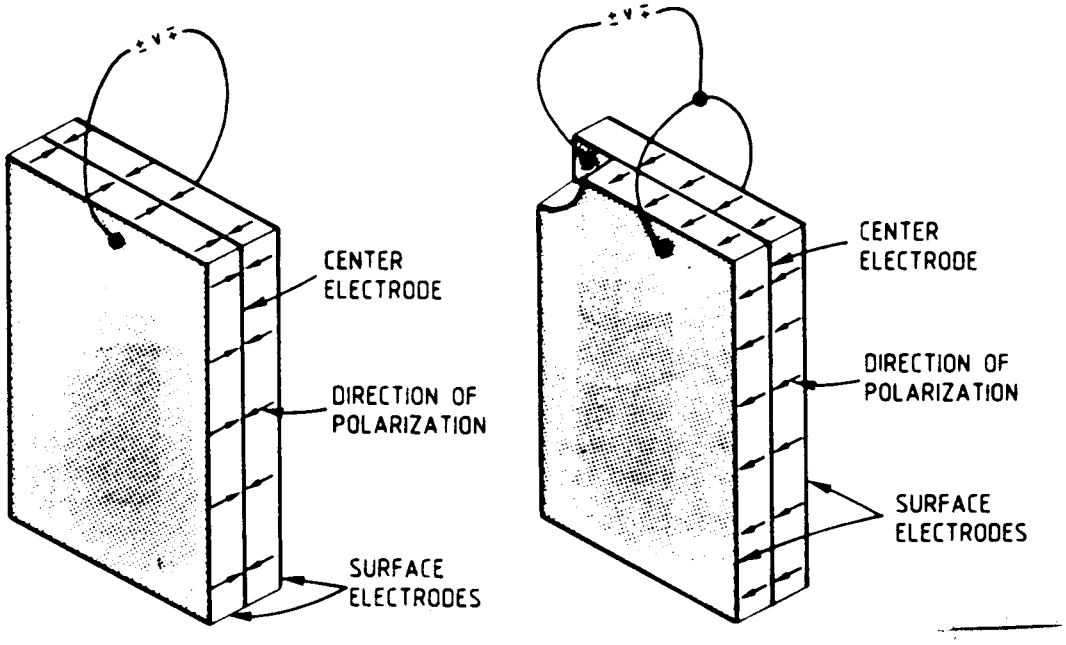

Figure 4.19 Different wiring setups for bender elements, (a) series connection, and (b) parallel connection (Dyvik and Madshus 1985).

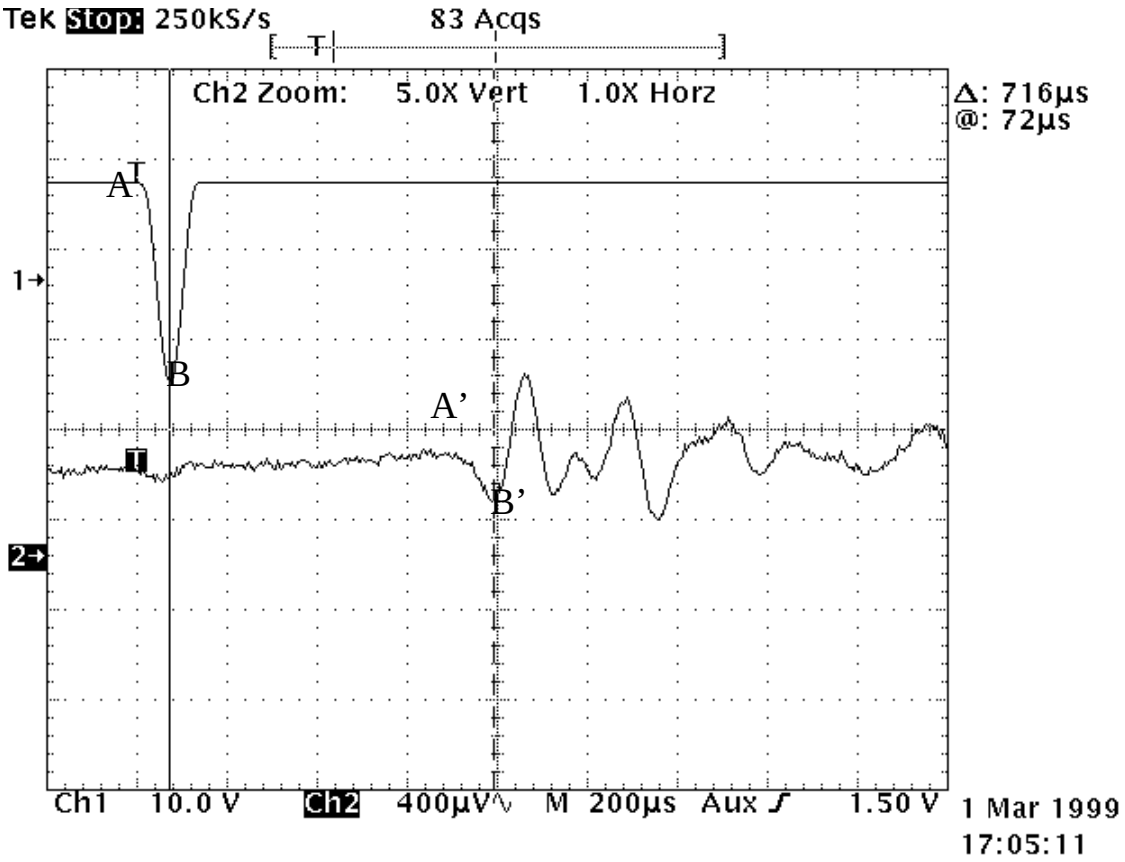

Figure 4.20 Oscilloscope screen image showing the transmitted half sine pulse and the received signal.

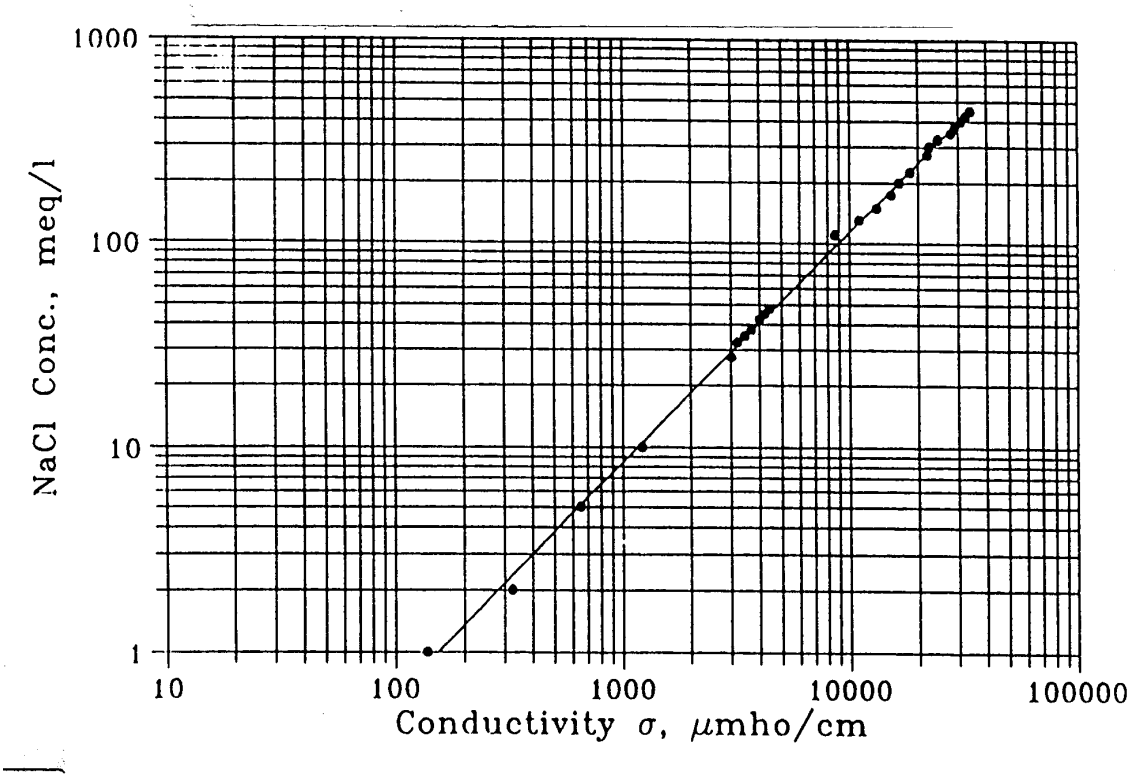

Figure 4.21 Influence of salt concentration on the electrical conductivity of water (Sadek 1993).

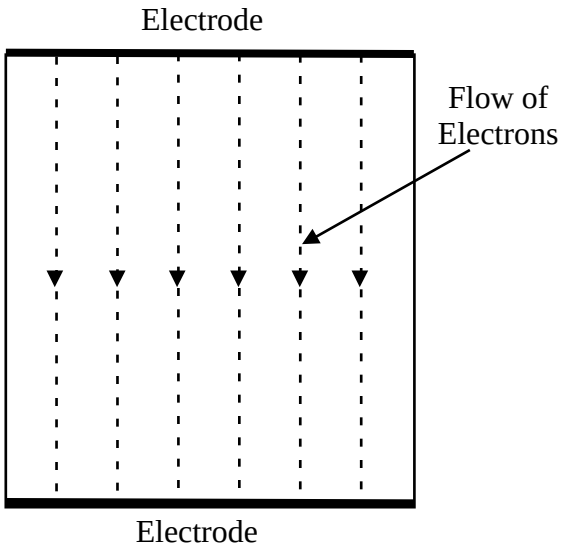

(a)

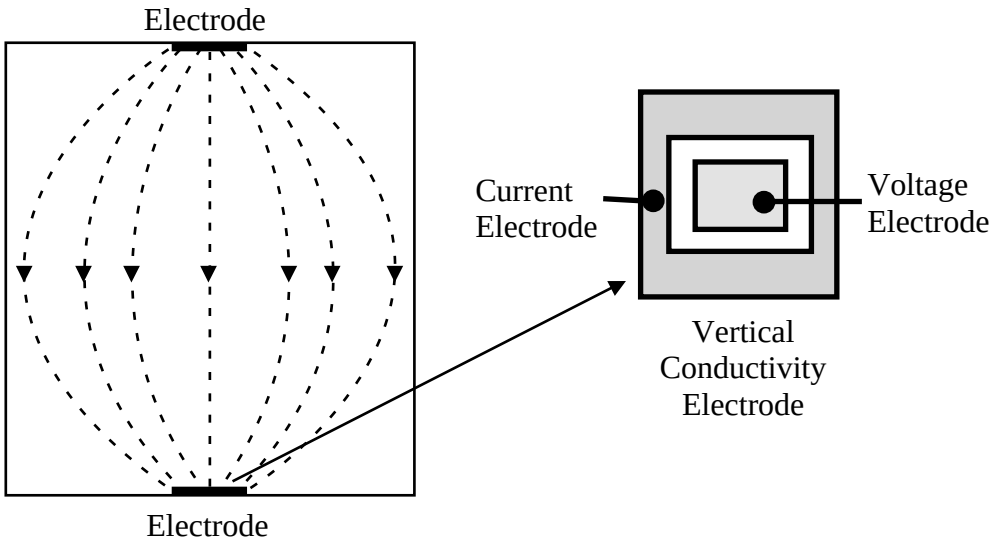

(b)

Figure 4.22 Flow of electrons through a sample for (a) 1-D conditions, and (b) 2-D conditions.

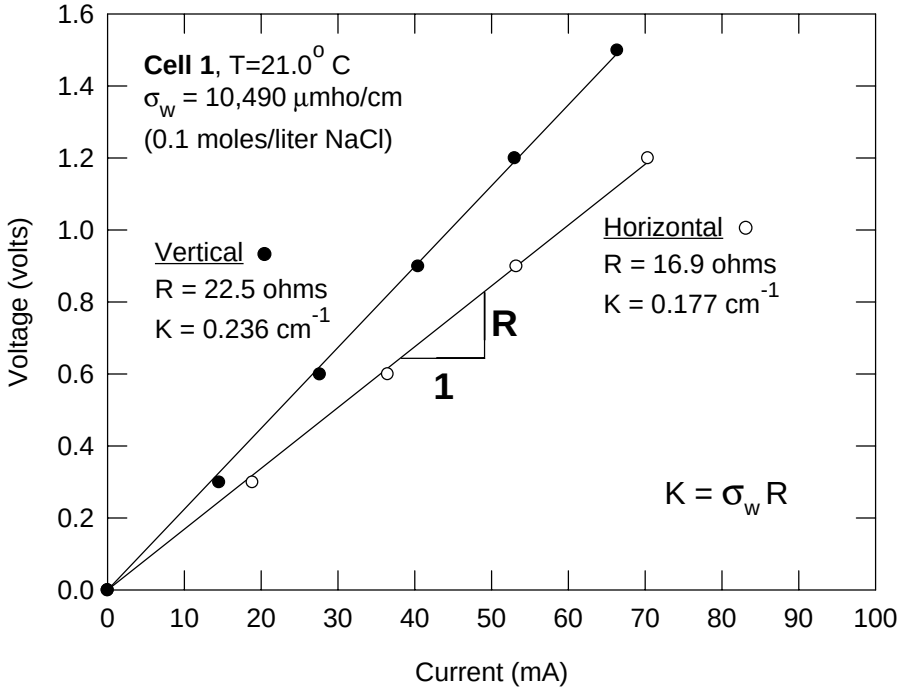

Figure 4.23 Determination of cell constants, K, for electrical conductivity.

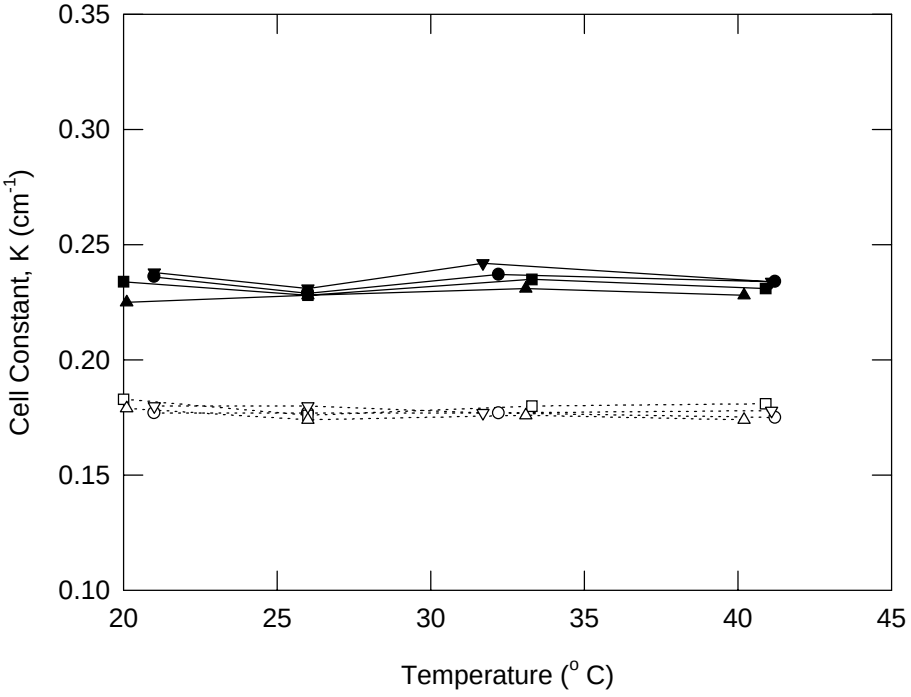

Figure 4.24 Variation of cell constant, K, with temperature.

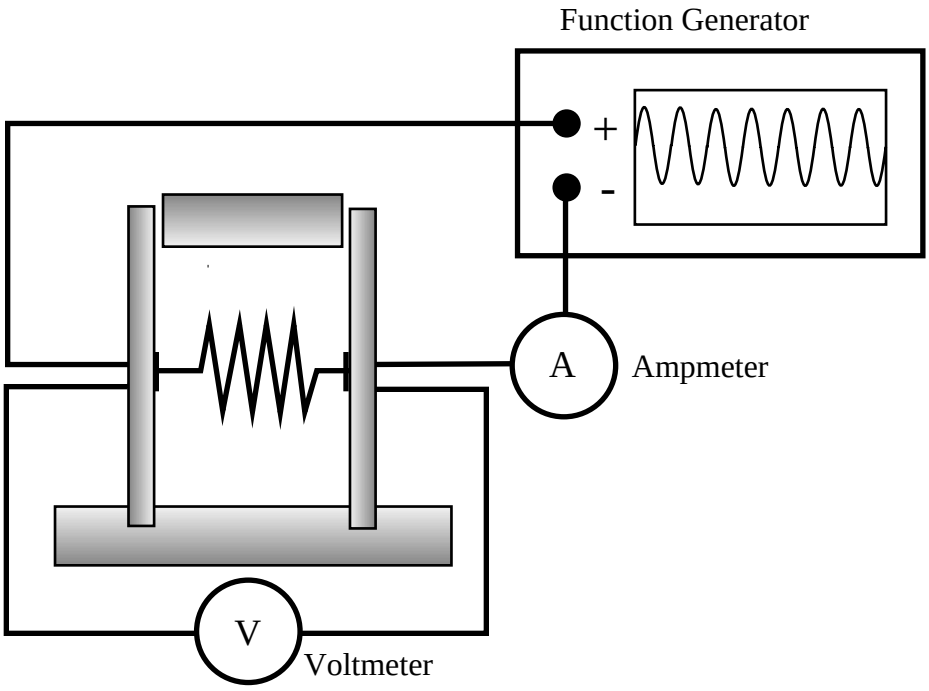

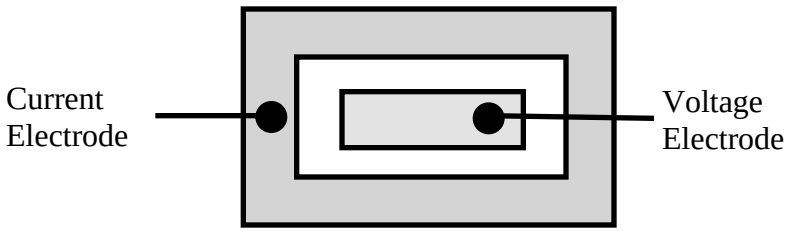

Horizontal Conductivity Electrode

Figure 4.25 Schematic of electrical conductivity setup.

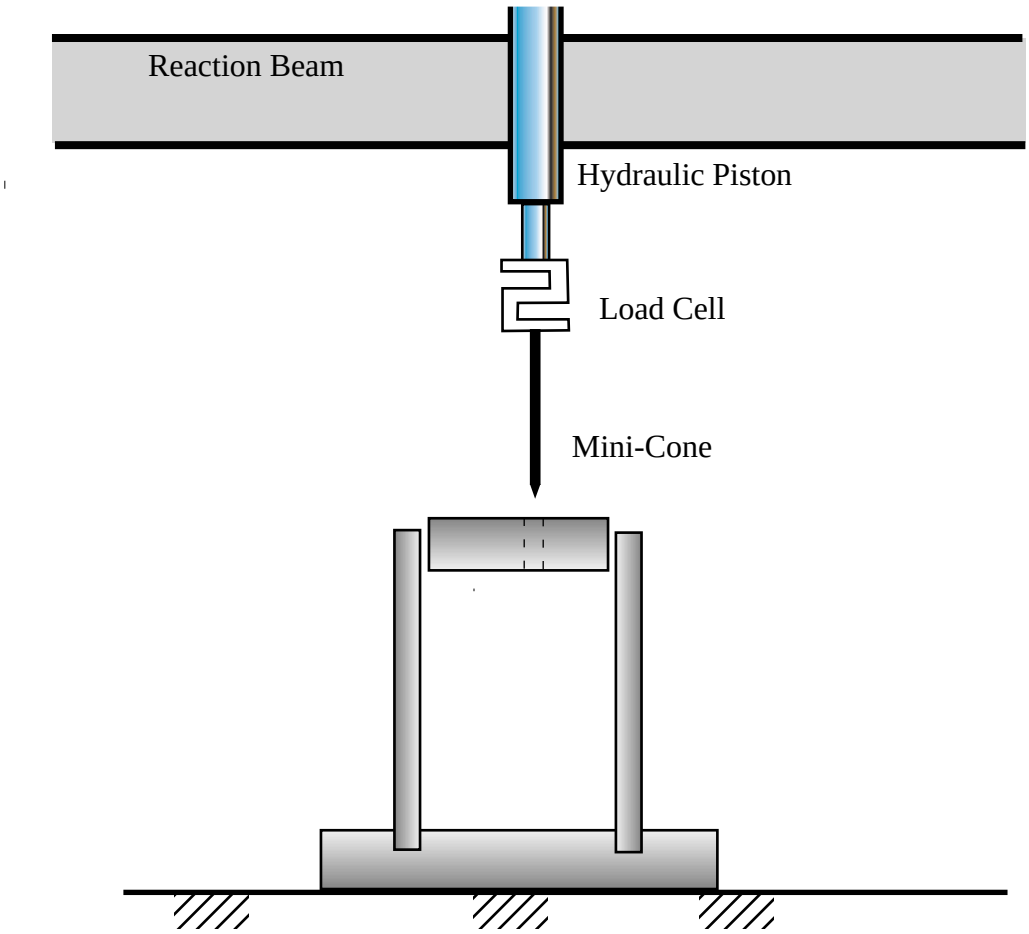

Figure 4.26 Schematic of mini-cone penetration tests.

Figure 4.27 PVC “extenders” used during pluviation of samples.

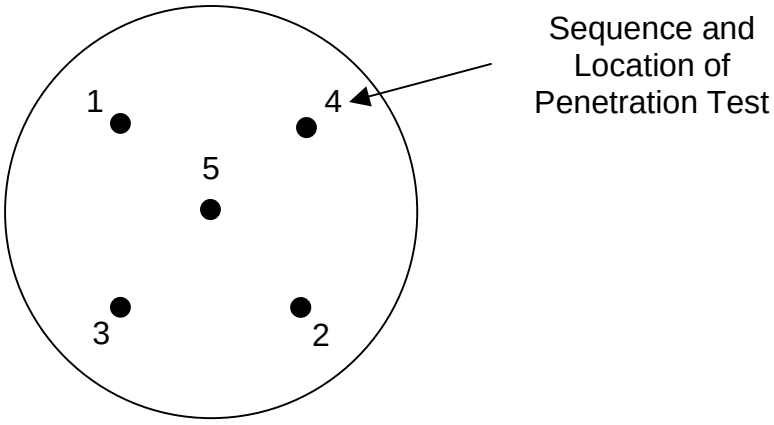

Figure 4.28 Mini-cone penetration test for bucket tests.